nature microbiology

Article

https://doi.org/10.1038/s41564-026-02279-6

A clinic-responder-derived defined microbial consortium enhances anti-PD-1 immunotherapy efficacy in mice

Received: 23 March 2025

Accepted: 26 January 2026

Published online: 09 March 2026

Check for updates

Haiyan Zhou[1,8], Ruiming Sun[2,3,8], Xiaoqun Nie[1,8], Liliang Xia[3,8], Hui Dong[4], Yujie Liu[1], Shurui Hou[5], Wenyue Dong[1], Xiaokuan Zhu[3], Yaxian Yao[3], Guo-Ping Zhao[5,6], Shun Lu[3] ✉, Ying Wang[2] ✉ & Chen Yang[1,7] ✉

Targeting the gut microbiota is a promising strategy to enhance the efficiency of cancer immunotherapy; however, success has been limited. Here we combined metagenomic analysis and in silico prediction to identify bacterial species associated with immunotherapy response in patients with non-small-cell lung cancer. We constructed a defined consortium (RCom) of 15 bacterial species, most of which were isolated from responder patient faeces, associated with improved clinical response to anti-programmed cell death protein 1 (PD-1) treatment. Metabolic models and in vitro experiments revealed that RCom is a stable and cooperative community, and in vivo experiments showed that RCom engrafts and produces immunom odulatory metabolites. Oral administration of RCom improved the anti-tumour activity of anti-PD-1 by increasing the intratumoural infiltration and cytotoxic function of $CD8^+$ T cells in syngeneic tumour models and across mice with heterogeneity in baseline gut microbiota composition. RCom supplementation also limited anti-PD-1 resistance in mice conferred by faecal microbiota transplantation from individual non-responsive patients. These findings suggest that RCom is a potential adjuvant to improve responsiveness to anti-PD-1 therapy in cancer.

Immune checkpoint inhibitors (ICIs) are established as effective treatments for a broad range of advanced cancers[1]. As the most widely used ICIs, antibodies targeting programmed cell death protein 1 (PD-1) and its ligand PD-L1 are highly efficacious against advanced melanoma, renal cell carcinoma and non-small-cell lung cancer (NSCLC)[2–4]. However, only a minority of patients showed durable clinical responses to ICIs[5,6]. ICIs can also cause immune-related adverse events that are severe in some cases[7]. Growing evidence supports a role for the gut microbiota in shaping anti-tumour immune responses during treatment with ICIs[8–10]. Many studies have shown that antibiotic treatments negatively affect patient response to ICIs[11,12]. Faecal microbiota transplantation (FMT) from patients who responded to ICIs into mice ameliorated the anti-tumour effect of ICIs, whereas FMT from non-responding patients failed to do so, thereby establishing a causal link between the gut microbiota and anti-tumour activity of ICIs[13–15]. Pilot clinical trials showed that FMT from patients who are responsive to anti-PD-1 may overcome resistance to PD-1 blockade therapy[16,17]. These findings strongly suggest that the gut microbiota is a promising therapeutic target of interventions designed to promote responsiveness to ICIs.

Strategies for targeting the gut microbiota in cancer immunotherapy include FMT, dietary interventions and administration of probiotics or defined microbial consortia[18–20]. Defined microbial consortia may better maintain an ecological balance within the gut microbiota than single-strain probiotics[21,22] and be more scalable, reproducible and

A full list of affiliations appears at the end of the paper. ✉e-mail: shunlu@sjtu.edu.cn; ywangssmu@shsmu.edu.cn; yang.c@sjtu.edu.cn

safe than FMT[23,24]. However, how to design and construct a microbial community with the desired immunomodulatory function remains a major challenge[25]. A consortium of 11 rare human-associated bacterial strains has been shown to induce interferon-γ (IFNγ)-producing $CD8^+$ T cells and enhance the anti-cancer activity of ICIs in mouse models[26]. This consortium was identified using a top-down gnotobiotic approach to narrow down the complex faecal microbiota from a healthy human by antibiotic treatment in mice[26]. Recently, three phase 1 and 2 trials combining microbial consortia with ICIs in patients with advanced-stage cancers have been conducted (NCT03686202, NCT03817125 and NCT04208958)[27–29]. The preliminary data indicate variable levels of microbial engraftment, which probably reflect the variations in the native microbiota of each patient[27,30]. Antibiotic use is unlikely to be a useful strategy for promoting engraftment by depleting the native microbiota without impairing the efficacy of ICIs[12,30,31]. Interindividual microbial heterogeneity thus remains a key hurdle for the design of clinic interventions capable of reproducibly modulating the microbiota.

In this study, we aimed to create a defined microbial consortium that is capable of reproducibly modulating the gut microbiota to enhance the anti-cancer efficacy of anti-PD-1 treatment. We started by rationally designing the bacterial community RCom with a bottom-up approach from the faecal microbiota of patients with advanced NSCLC who responded to anti-PD-1 immunotherapy. Through in vitro assembly and characterization, the RCom was revealed as a stable and relatively cooperative community. We then supplemented the RCom by oral gavage to mice, showing that the RCom members act together to establish optimal engraftment and produce immunomodulatory metabolites. Oral administration of the RCom increased the anti-tumour activity of anti-PD-1 in multiple tumour models despite a profound heterogeneity of the baseline gut microbiota. Finally, we showed that supplementation of RCom restored the therapeutic efficacy of anti-PD-1 in mice with FMT from ICI-refractory patients. These results suggest the potential clinic utility of our developed consortium in improving the efficacy of ICI immunotherapy.

Results

Designing a clinic-responder-derived bacterial community

To design a microbial consortium for modulating gut microbiota and ultimately improving responsiveness to PD-1 blockade therapy, we examined the gut microbiome of 59 patients with advanced NSCLC who received anti-PD-1 treatment (Fig. 1a and Extended Data Fig. 1a). Patients with partial response or stable disease lasting at least 6 months after treatment initiation were classified as responders, whereas those with progressive disease or stable disease lasting less than 6 months were classified as non-responders (Supplementary Table 1)[14]. To determine the gut bacterial species that were most prevalent and enriched in responders, we performed metagenomic shotgun sequencing on faecal samples collected from patients before starting the therapy (Fig. 1b). The enrichment of bacterial species in responders versus non-responders was compared using linear discriminant analysis (LDA) of effect size (LEfSe). A total of 16 species were found to meet the criteria of LDA score of 3.0 or more and a prevalence of 1.0 (occurring in all the responders) (Extended Data Fig. 1a,b).

Beyond promoting therapeutic responsiveness, modulation of the gut microbiota is also expected to improve the safety of ICI treatment[19]. The microbial signatures in patients with cancer, which are associated with immune-related adverse events (irAEs) during treatment with ICIs, have been reported[32,33]. Thus, we removed one species (*Bacteroides intestinalis*) that showed a higher abundance in patients with severe (at least grade 3) irAEs (Extended Data Fig. 1b). In addition, we searched all the available genomes for each species and removed three species with most genomes encoding prominent virulence factors, toxins or multidrug resistance (Extended Data Fig. 1b and Supplementary Tables 2 and 3).

We next sought to enhance the engraftment capability of the designed bacterial consortia. Beneficial intracommunity interactions have been shown to be critical for natural microbial communities to persist across multiple hosts[34,35]. However, it remains largely to be explored whether interspecies interactions could be used to design synthetic microbial consortia for modulation of host-associated microbiota[36]. We assessed the extent of potential resource competition and metabolic dependencies in the synthetic bacterial communities using genome-scale metabolic models (GEMs) for individual species[37] and the species metabolic interaction analysis (SMETANA) tool[38] (Extended Data Fig. 1c). As the presence of multiple species from the same genus may increase the risk for resource competition within the community, *Roseburia intestinalis* was removed, resulting in 11 species as core members of the designed community (Fig. 1b and Extended Data Fig. 1c). These species could interact with other bacterial species in the gut microbiota of responders. We hypothesized that intracommunity metabolic cooperation may facilitate the persistence of synthetic microbial communities across multiple hosts. Thus, additional members were examined based on simulations of community metabolism. The candidates included the bacterial species that were abundant in responders (relative abundance of 1% or more on average) but did not show significantly different abundance between responders and non-responders. *Dorea formicigenerans*, *Alistipes finegoldii* and *Alistipes inops* were also included in the simulations because they were found to be associated with reduced risk of developing severe irAEs[33]. These species were individually or combinatorially grouped with the 11 core members, generating 511 bacterial communities with sizes ranging from 12 to 20 (Extended Data Fig. 1c). For all these communities, we computed the metabolic resource overlap (MRO) score and SMETANA score (Supplementary Table 4), which provide a measure of potential metabolic competition and cooperation, respectively[38]. Among the communities that have higher SMETANA scores and lower MRO scores, a community of 15 bacterial species (termed 'RCom') was selected for further studies (Extended Data Fig. 1c).

The RCom consists of 5 Bacteroidetes and 10 Firmicutes species (Fig. 1b). Cross-feeding interactions between these species were predicted from the simulations (Fig. 1c). Notably, the interactions between the Firmicutes and Bacteroidetes species in the RCom were about 5 times more frequent than those in the 11 core members (Extended Data Fig. 1d), suggesting an enhancement of interphylum interactions in the RCom. Among these interactions, the cross-feeding with the Firmicutes as receivers and Bacteroidetes as donors was predominant (Fig. 1c). The metabolites predicted to be most exchanged in the RCom were amino acids (Extended Data Fig. 1e,f), which is consistent with previous experimental observations of amino acid exchange in natural microbial communities[39].

The cumulative abundance of the 15 bacterial species is significantly associated with progression-free survival (PFS) in the anti-PD-1-treated NSCLC cohort (hazard ratio (HR) 0.519, 95% confidence interval (CI) 0.276–0.975, $P = 0.041$) (Supplementary Fig. 1a). To assess whether the RCom abundance correlates with clinical outcomes of ICIs in independent cohorts, we analysed two previously published cohorts of ICI-treated patients with NSCLC ($n = 476$, PRJNA1023797; $n = 325$, PRJNA751792)[40,41]. Median overall survival (OS) of patients having high abundance of the RCom is significantly prolonged compared with patients having low abundance of the RCom (18.8 months versus 13.5 months, HR 0.735, 95% CI 0.604–0.894, $P = 0.0001$) (Fig. 1d and Supplementary Table 5). Among the 15 species, at least 5 are more abundant in responder patients in both cohorts (Supplementary Fig. 1b). We also evaluated the abundance of the 15 species in an additional cohort of anti-PD-1-treated patients with advanced renal cell carcinoma or NSCLC ($n = 187$, PRJEB22863)[13], showing that 8 species are enriched in responders (Supplementary Fig. 1b). Thus, the RCom comprises a number of species that are consistently associated with improved response to ICI treatment in patients with cancer.

https://doi.org/10.1038/s41564-026-02279-6

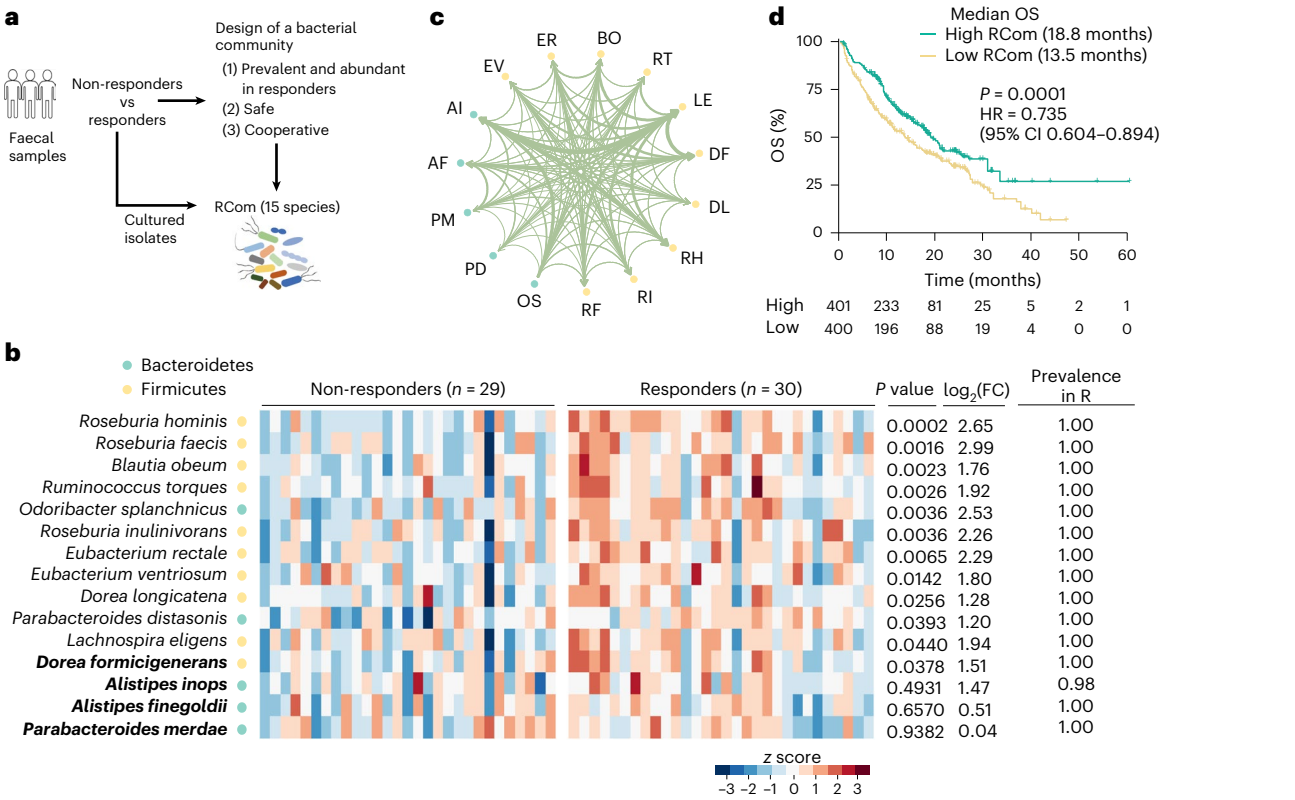

Fig. 1 | A defined bacterial consortium derived from clinic responders to anti-PD-1 treatment. a, Schematic showing the design and construction of the 15-member community RCom. **b**, Relative abundance of the 15 bacterial species in responders versus non-responders among anti-PD-1-treated patients with NSCLC as determined with metagenomic shotgun sequencing on faecal samples. Coloured circles indicate the phylum of each species. The species in bold were added to the community based on potential metabolic cooperation. Heat map colours represent the *z*-score (red and blue indicate high and low abundance, respectively). Statistical significance was calculated by two-tailed Mann–Whitney *U* test. FC, fold change. The prevalence of each bacterial species in the responders (R) is also shown. **c**, Predicted cross-feeding interactions between the RCom members (denoted by two-letter abbreviations). The edge width represents the frequency of each interaction. **d**, Kaplan–Meier plot of OS in ICI-treated patients with NSCLC according to cumulative abundance of the 15 species in independent cohorts. *P* values for survival differences were calculated using the two-sided log-rank test. HR and 95% CI were estimated from the stratified Cox proportional hazards regression model.

To isolate the RCom members from the responder microbiota, diluted faecal samples from 4 patients responsive to anti-PD-1 (Supplementary Table 6) were cultured on 14 different media (Supplementary Table 7), which allowed us to isolate 10 species of the community (Extended Data Fig. 2a,b). Multiple strains were detected for these species, which agrees with their highly variable genomes as shown by a recent study[42]. To reduce intraspecies competition, we selected a relatively rapidly growing strain from the cultured isolates for each of the 10 species. The remaining 5 species of the community were obtained from public collections. Thus, a consortium of 15 species was constructed for experimental characterization. For comparison, we also assembled 13 bacterial species that were isolated from non-responder patients (Extended Data Fig. 2c).

RCom is a stable and cooperative community

Stability is a key factor to consider when designing bottom-up microbial communities[21]. To examine whether the RCom is stable in vitro, we studied the effect of different inoculation ratios on community composition (Fig. 2a). We cultured the bacterial community on a chemically defined medium (Supplementary Table 8) and determined the abundance of each member by quantitative PCR (qPCR) (Supplementary Table 9). The community reached a stable configuration by 48 h, with the range of cell densities for different species spanning 4 orders of magnitude (Extended Data Fig. 3a). In addition to equal ratio for each of the 15 species, we tested 2 other inoculation ratios, which are directly and inversely proportional to the growth rate of each species, respectively (Fig. 2a and Supplementary Table 10). After 48 h of cultivation, the communities generated from 3 different inoculation ratios had a nearly identical composition (Fig. 2b). Thus, the steady-state community composition was stable despite dramatic changes to inoculation ratios. We hypothesized that the stability of the RCom results from the interactions between members. We compared the utilization of various carbohydrates by the RCom members. The 15 bacterial species were found to differ in their preferences for the substrates tested (Extended Data Fig. 3b), suggesting that these species partition their niches, thereby reducing interspecies competition.

To identify interspecies interactions in the RCom, we performed pairwise co-cultures for the 15 bacterial species and compared the growth of individual species between co-cultures and monocultures (Fig. 2c). The medium used was a chemically defined medium containing all the essential components for growth of each species (Supplementary Table 8). Either positive or low-level competitive interactions between the species were detected (Fig. 2d), with a significantly higher degree of positive interactions (Fig. 2e). This is consistent with the GEM-based simulation results of interspecies interactions described above. Among the 48 positive interactions detected, 16 were mutualistic interactions between Firmicutes and Bacteroidetes species, and 9 were commensal interactions that benefit Firmicutes species and are neutral to Bacteroidetes species (Fig. 2f). Almost all the Firmicutes species gained fitness advantages from interactions with at least one Bacteroidetes species in the RCom (Fig. 2d).

https://doi.org/10.1038/s41564-026-02279-6

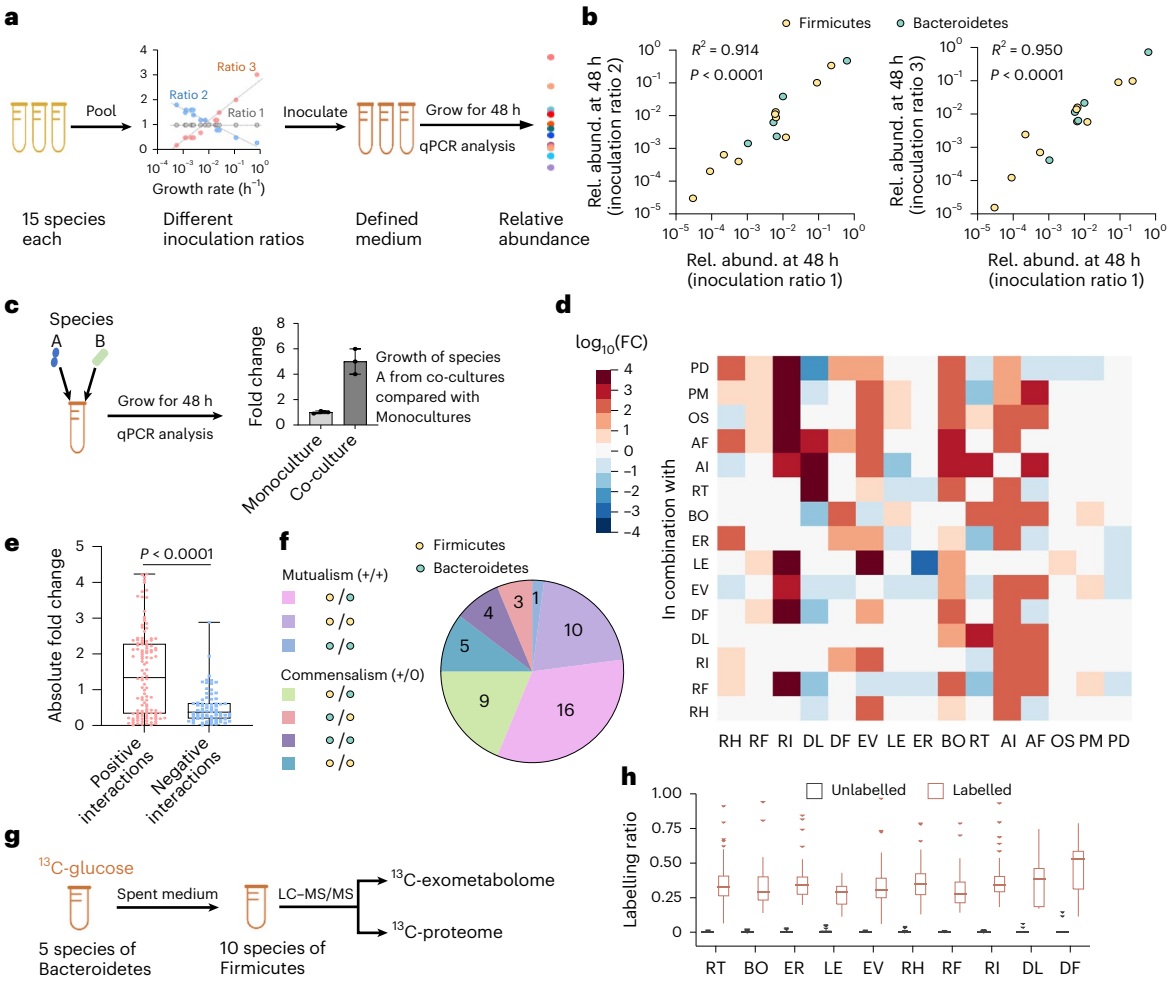

Fig. 2 | RCom is a stable and cooperative community. a, Schematic of the inoculation shift experiment. Three different inoculation ratios were tested: ratio 1 denotes the same ratio for each of the 15 bacterial species, and ratios 2 and 3 are inversely and directly proportional to the growth rate of each species, respectively. **b**, Communities generated from 3 different inoculation ratios have a nearly identical composition at 48 h. The colour of each circle represents the phylum of the corresponding species. Data shown are mean values from three independent experiments. Correlation was assessed using two-tailed Pearson's test. The R^2 and P values are shown. Rel. abund., relative abundance. **c**, Schematic of the pairwise co-culture experiment. Data shown are mean values and s.e.m. ($n = 3$ independent experiments). **d**, Pairwise co-cultivation of the RCom members for 48 h. The abundance of each species from three independent experiments was averaged and normalized to that from monocultures. The resulting fold change ($\log_{10}$ transformed) is shown. See Extended Data Fig. 3a for abbreviations of the RCom members. **e**, Box plots showing the absolute $\log_{10}$-transformed fold changes in species abundance. Values represent the mean from three independent biological replicates, comparing pairwise co-cultures with their respective monocultures. The plots depict the minimum and maximum values (whiskers), the upper and lower quartiles, and the median. P values were calculated using two-tailed Mann–Whitney U test. **f**, Number of mutualistic and commensalistic interactions between RCom members. **g**, Schematic for detecting metabolic cross-feeding between Bacteroidetes and Firmicutes species in the RCom. **h**, ^{13}C-labelling ratio of peptides from each species after 12 h of cultivation of the 10-Firmicutes-species community. Data shown are from three independent biological replicates from ^{13}C-labelled (orange) and unlabelled (black) spent medium experiments. The box plots depict the median, the upper and lower quartiles, and the rest of the distribution. Points that are 1.5 times the interquartile range beyond the upper and lower quartiles are considered outliers and shown individually. Complete data are shown in Extended Data Fig. 4b.

We used ^{13}C isotope tracing in combination with liquid chromatography–mass spectrometry (LC-MS)-based meta-proteomics and exometabolomics to elucidate the metabolic dependencies of Firmicutes species on Bacteroidetes species in the RCom (Fig. 2g). Five Bacteroidetes species were grown on the defined medium lacking amino acids and supplemented with ^{13}C-glucose for 12 h, during which glucose in the medium had been just exhausted. The spent medium was added to the culture of the 10-Firmicutes-species community. Extracellular ^{13}C-labelled and unlabelled metabolites were quantified using a targeted metabolomics approach[43]. We observed that the extracellular concentrations of ^{13}C-labelled amino acids including glycine, serine, lysine, histidine, tryptophan and proline decreased after 6 h of cultivation (Extended Data Fig. 4a), suggesting that these amino acids were produced by the Bacteroidetes species and consumed by the Firmicutes species. Furthermore, we analysed the ^{13}C incorporation into each of the Firmicutes species using a ^{13}C-based proteomics method[44]. The labelled and unlabelled peptides were assigned to each species based on reference peptides from samples of unlabelled amino acid-supplemented cultures (Supplementary Table 11). The degree of ^{13}C labelling in each species-specific peptide was quantified. We found that the labelling degree in the peptides of each Firmicutes species was considerably increased compared with that in the unlabelled spent media-supplemented cultures (Fig. 2h and Extended Data Fig. 4b). This result indicates that the Bacteroidetes-supplied amino acids were used for protein synthesis by each of the Firmicutes species. In addition, we observed an increase in the extracellular concentrations of many metabolites including butyrate, butyrylglycine, ATP, inosine monophosphate (IMP), hypoxanthine and inosine in the cultures of the

10-Firmicutes-species community (Extended Data Fig. 4c). Together, these in vitro experimental results show that the RCom is a relatively cooperative community, in which amino acids are involved in the dependency of the Firmicutes species on the Bacteroidetes species.

RCom supplementation shapes intestine immune responses

To determine whether the RCom has immunomodulatory functions, we supplemented specific-pathogen-free (SPF) mice with the bacterial community by oral gavage (Fig. 3a). First, we evaluated the engraftment of the RCom in mice (Extended Data Fig. 5). Following oral administration, the abundances of all the 15 species in faeces were increased within 6 h and then significantly decreased after 24 h (Supplementary Fig. 2a), suggesting that daily administration of the RCom is required. We then supplemented mice with the RCom or phosphate-buffered saline (PBS) daily for 7 days and analysed the immune responses of colonic lamina propria cells using flow cytometry (Extended Data Fig. 6 and Supplementary Table 12). Notably, the RCom-fed mice showed a remarkably increased percentage of $CD8^+$ T cells expressing IFNγ, tumour necrosis factor (TNF), granzyme B (GzmB) and CD107a in the colon but not in the spleen (Fig. 3b,c and Extended Data Fig. 6a-d). These results indicate that RCom administration induced the cytotoxic function of $CD8^+$ T cells in the gut. The induction capability of the RCom was not confined to $CD8^+$ T cells, but extended to $CD4^+$ T cells as well (Extended Data Fig. 6e). RCom supplementation also resulted in a decreased population of regulatory T (T_{reg}) cells but an increased population of natural killer (NK) cells in the colonic lamina propria of mice (Extended Data Fig. 6a). By contrast, we did not observe any significant responses of colonic $CD8^+$ T cells in mice supplemented with the non-responder-derived 13 bacterial species (13-mix) (Supplementary Fig. 3a).

We tested the immunomodulatory effect of RCom subsets including only the 5 Bacteroidetes species (5-mix), only the 10 Firmicutes species (10-mix-I) and 2 cross-phylum combinations (10-mix-II and 10-mix-III) (Extended Data Fig. 2b). All of these RCom subsets failed to induce the cytotoxic activity of colonic $CD8^+$ T cells in mice (Fig. 3c, Extended Data Fig. 6c,f and Supplementary Fig. 3b). No induction was also observed after treating mice with heat-killed RCom (Extended Data Fig. 6g and Supplementary Fig. 3c). We observed that supplementation with the RCom enhanced the expression of CD80, major histocompatibility (MHC) class I and interleukin-12 (IL-12) on colonic lamina propria dendritic cells (DCs) in mice (Extended Data Fig. 6h and Supplementary Fig. 3d). By contrast, all the RCom subsets were incapable of stimulating IL-12 production by colonic DCs (Extended Data Fig. 6h). This result is consistent with the hypothesis that the RCom may induce $CD8^+$ T cell response via a DC-dependent mechanism. Indeed, several commensal bacteria have been shown to be capable of promoting T cell responses by modulating the activation and maturation of DCs[8,13,45]. Thus, our results suggest that the live species of the RCom act together to boost the cytotoxic function of colonic $CD8^+$ T cells in mice.

We examined the composition of caecal microbiota, which showed that supplementation of the 5-mix increased the relative abundance of the 5 Bacteroidetes species (Extended Data Fig. 5a). Thus, these Bacteroidetes species, even with high abundance, were not sufficient for immunomodulation. However, the 10 Firmicutes species showed much lower abundance in the 10-mix-I-fed mice than the RCom-fed mice (Extended Data Fig. 5a). The abundance of several of these species was even not increased by the 10-mix-I supplementation. This result showed limited levels of engraftment of the Firmicutes species in the absence of the 5 Bacteroidetes species in the RCom, which is consistent with the observed metabolic dependencies of the former on the latter species. Indeed, we observed an increased abundance of some of the Firmicutes species by the presence of the 5 Bacteroidetes species in the 10-mix-II- or 10-mix-III-fed mice (Supplementary Fig. 2b). This is consistent with the idea that successful engraftment of the 10 Firmicutes in the RCom appears necessary for immunomodulation. In addition, we performed metabolomic profiling of caecal samples from mice supplemented with RCom or its subsets. A number of metabolites including butyrate, acetate, inosine, hypoxanthine and IMP showed increased levels in the RCom-fed mice compared with the subset-fed mice (Extended Data Fig. 5b).

Substantial evidence exists that an individual's baseline microbiota influences the success of microbiota-targeting interventions[46,47]. To test the engraftment capability of the RCom in mouse models possessing a variety of pre-existing gut microbiota, we used four cohorts of SPF mice obtained from different commercial suppliers or the same supplier but in separate shipment batches. Consistent with previous findings[48,49], mice from different batches or suppliers varied substantially in their baseline gut microbiota (Extended Data Fig. 7a–c). We supplemented the four cohorts of mice with the RCom and determined the colonic $CD8^+$ T cell response. RCom supplementation induced production of IFNγ, TNF, GzmB and CD107a by colonic $CD8^+$ T cells from all the four cohorts of mice (Fig. 3d), indicating that the immunomodulatory effect of the RCom was not influenced by the baseline gut microbiota.

For each of the four mouse cohorts with different baseline microbiota, the relative abundance of most of the 15 species was increased in the caecal microbiota of RCom-fed mice (Extended Data Fig. 7d). However, the respective species and their increased abundances were not the same in different cohorts. Indeed, the RCom-fed mice from different cohorts showed distinct microbiome composition, as the baseline microbiota seems to exert a bigger effect on the microbial composition than the RCom supplementation (Extended Data Fig. 7e). An appealing hypothesis is that supplementation of the RCom induces the same functions of the gut microbiome despite the variety of microbial composition. To identify the microbial metabolic processes and products influenced by RCom supplementation, we performed metagenomic shotgun sequencing and metabolomic analysis on caecal samples from two cohorts of mice that were obtained from different commercial suppliers. Functional profiling from metagenome-assembled genomes (MAGs) revealed several metabolic modules including butyrate synthesis via butyryl-co-enzyme A transferase (route I) and via butyrate kinase (route II) and degradation of methionine, histidine, proline and adenine ribonucleotide, which were enriched in the RCom-supplemented mice from both cohorts (Fig. 3e, Extended Data Fig. 7f and Supplementary Table 13). In fact, degradation of methionine, histidine and proline may lead to production of crotonyl-co-enzyme A that is further converted to butyrate (Extended Data Fig. 7g)[50]. Adenine ribonucleotide degradation could produce purine metabolites including IMP, inosine and hypoxanthine[51]. In addition, the biosynthetic modules for tryptophan and vitamins (pantothenate, biotin and tetrahydrofolate) were also enriched in the caecal microbiome of RCom-supplemented mice from both cohorts (Extended Data Fig. 7f). Interestingly, we found that the same metabolic modules enriched in the RCom-fed mice were encoded by the genomes of distinct bacteria in the two cohorts (Fig. 3e, Extended Data Fig. 7f and Supplementary Table 14). Thus, supplementation of the RCom to different baseline microbiota increased abundance of the bacterial species that were taxonomically different but shared the same metabolic functions, showing the functional redundancy and stability of the RCom-supplemented gut microbiota. Consistent with the findings of functional metagenomics, metabolomic profiling of caecal contents showed increased concentrations of butyrate, acetate, inosine, hypoxanthine and IMP in the RCom-fed mice from both cohorts (Fig. 3f and Supplementary Fig. 4), suggesting a potential mechanistic role. Indeed, previous studies have shown that butyrate and inosine produced by gut bacteria can enhance $CD8^+$ T cell cytotoxicity[45,52]. Collectively, these findings indicate that RCom supplementation shapes metabolites produced by gut microbiota and promotes activation of cytotoxic $CD8^+$ T cells.

https://doi.org/10.1038/s41564-026-02279-6

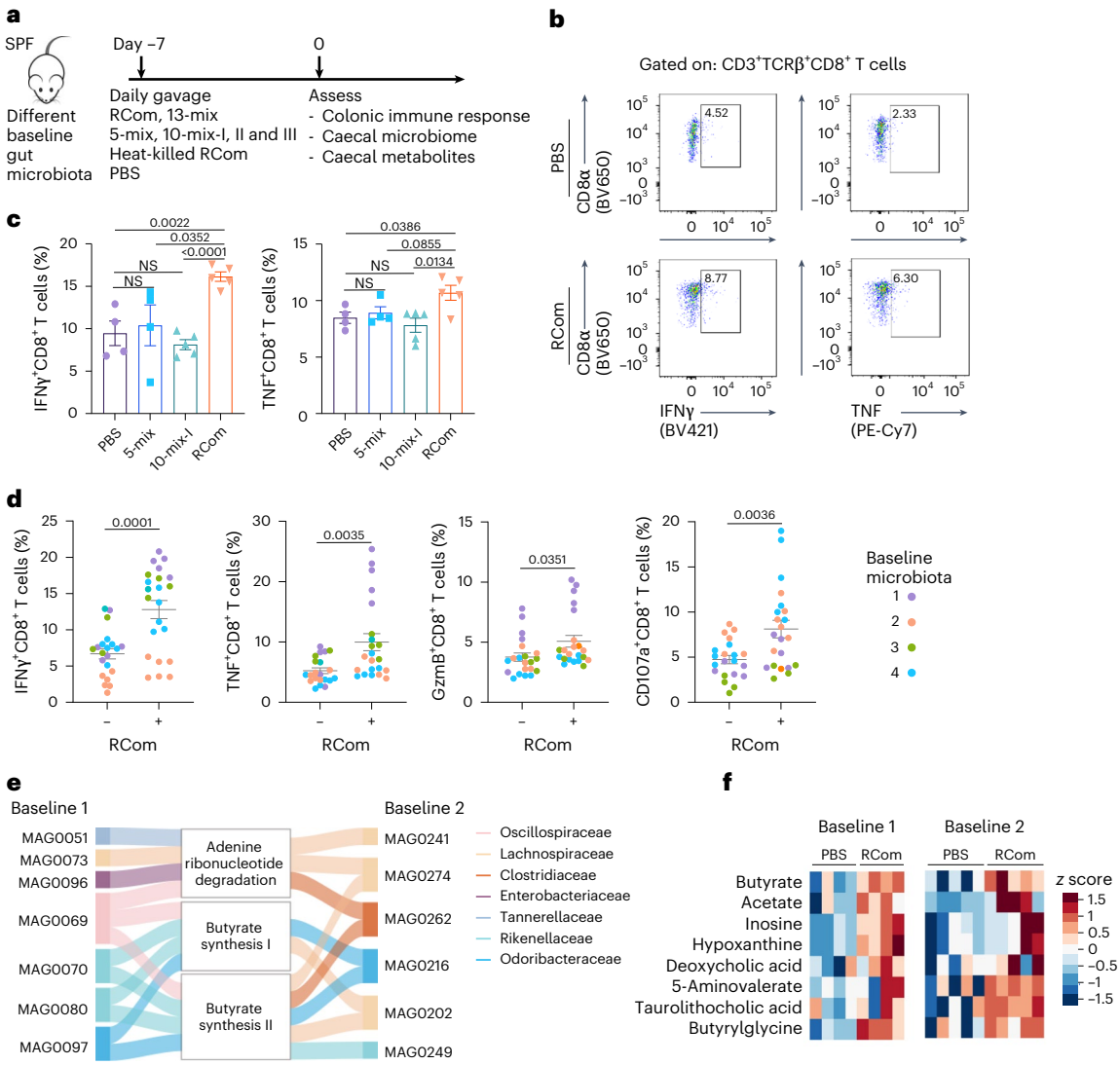

Fig. 3 | RCom supplementation shapes intestine microbiome functions and immune responses. a, Schematic of the experimental set-up. SPF C57BL/6 mice were supplemented with the indicated bacterial mixtures or PBS daily by oral gavage for 7 days. **b**, Representative flow cytometry plots showing the expression of IFNγ and TNF by CD8$^+$ T cells in the colonic lamina propria isolated from RCom- and PBS-fed mice from two independent experiments. **c**, Percentages of colonic IFNγ$^+$ and TNF$^+$ cells among CD8$^+$ T cells from mice supplemented with RCom ($n = 5$), its subsets 5-mix ($n = 4$) and 10-mix-I ($n = 5$), or PBS ($n = 4$). **d**, Four cohorts of SPF mice with different baseline gut microbiota were orally supplemented with RCom or PBS. Percentages of IFNγ$^+$, TNF$^+$, GzmB$^+$ and CD107a$^+$ of colonic CD8$^+$ T cells were determined. Each circle represents an individual mouse. **e**, Metabolic modules and their encoding MAGs enriched in RCom- versus PBS-supplemented mice from two cohorts with different baseline microbiota. MAGs were taxonomically classified according to NCBI RefSeq. Complete data are shown in Extended Data Fig. 7f. **f**, Heat map showing elevated metabolites in the caecal content of RCom- versus PBS-fed mice from the two cohorts. Complete data are shown in Extended Data Fig. 7h. Baseline 1: PBS, RCom, $n = 6$ mice per group; baseline 2: PBS, RCom, $n = 5$ mice per group; baseline 3: PBS, RCom, $n = 5$ mice per group; baseline 4: PBS, RCom, $n = 4$ mice per group. Data in **c** and **d** are mean values and s.e.m. Two-tailed unpaired *t*-test. NS, not significant.

RCom administration enhances anti-PD-1 efficacy in mice

We next evaluated whether administration of the RCom could boost the efficacy of PD-1 blockade treatment in tumour mouse models. First, we tested whether the combination of RCom supplementation and administration of an anti-PD-1 antibody (in the absence of tumours) could lead to systemic immune responses (Extended Data Fig. 8a). Indeed, RCom supplementation, when combined with anti-PD-1 treatment, significantly increased the DC population and production of IFNγ and TNF by CD8$^+$ T cells in the spleen of mice compared with heat-killed RCom-fed mice (Extended Data Fig. 8b). Thus, RCom administration induced systemic CD8$^+$ T cell activation in the presence of anti-PD-1. We then examined the effect of prophylactic RCom supplementation on anti-PD-1 treatment in tumour mouse models. SPF mice were daily supplemented with the RCom before inoculation of Lewis lung carcinoma (LLC) cells, and tumour growth was monitored with or without administration of an anti-PD-1 antibody. Mice with RCom supplementation and anti-PD-1 treatment showed significantly reduced tumour size compared with mice with the anti-PD-1 only (Fig. 4a), demonstrating that RCom administration increases the anti-tumour activity of anti-PD-1. By contrast, no enhancement of anti-PD-1 efficacy was observed for mice supplemented with the 13-mix (Extended Data Fig. 8c,d). Notably, supplementation of the RCom in the absence of anti-PD-1 was unable to inhibit tumour growth (Fig. 4a), showing that the anti-tumour effect of the RCom was dependent on anti-PD-1 treatment.

We observed that infiltration of CD8$^+$ T cells into the tumour was significantly higher in mice treated with RCom plus anti-PD-1 than mice with anti-PD-1 only (Fig. 4b). Accordingly, tumours from mice with combined treatment of RCom and anti-PD-1 revealed an increase in the population of total CD8$^+$ T cells and activated CD8$^+$ T cells (Extended Data Fig. 8f). Moreover, RCom supplementation enhanced

cytotoxic CD8$^+$ T cell function as evidenced by increased frequencies of IFNγ$^+$, TNF$^+$, GzmB$^+$ and CD107a$^+$ within CD8$^+$ T cells in the tumour and spleen (Extended Data Fig. 8g and Supplementary Fig. 5a). In addition, the proportion of IL-12$^+$ DCs in the tumour was increased by RCom supplementation (Fig. 4c). To assess the role of CD8$^+$ T cells and DCs in the anti-PD-1-promoting effect of the RCom, we treated mice with an anti-CD8 antibody to specifically deplete CD8$^+$ T cells or injected diphtheria toxin to deplete DCs. The beneficial effect of the RCom was completely abrogated in the mice depleted in CD8$^+$ T cells (Fig. 4d). Depletion of DCs significantly diminished the positive effect of the RCom on cytokine production by splenic and intratumoral CD8$^+$ T cells (Fig. 4e, Extended Data Fig. 8h and Supplementary Fig. 5b), suggesting that DCs are required for stimulating the CD8$^+$ T cell responses. Thus, the anti-PD-1-enhancing effect of the RCom is dependent primarily on CD8$^+$ T cells, probably mediated by triggering DC activation. Supplementation with subsets (5-mix and 10-mix-I) of the RCom failed to improve the efficacy of anti-PD-1 treatment or elicit anti-tumour immunity (Extended Data Fig. 8e,g). Collectively, these results suggest that the RCom species act together to enhance anti-PD-1-induced anti-tumour immunity in a CD8$^+$ T cell-dependent manner.

We tested whether the RCom could enhance the anti-PD-1 efficacy in other cancer models. Administration of the RCom was found to remarkably increase the anti-tumour activity of anti-PD-1 in the B16-F10 melanoma and MC38 colorectal cancer models (Fig. 4f,g). Significant improvement of the anti-PD-1 treatment by the RCom was also observed for additional lung cancer models including CMT-167 adenocarcinoma and ASB-XIV squamous carcinoma (Extended Data Fig. 8i,j). To examine whether the RCom could synergize with anti-PD-1 in mice with existing tumours, we supplemented SPF mice with the RCom by oral gavage 3 days after tumour inoculation (Fig. 4h). Therapeutic supplementation of RCom in combination with anti-PD-1 treatment significantly suppressed the growth of LLC or B16-F10 tumours in mice compared with anti-PD-1 only (Fig. 4i,j).

To examine whether the heterogeneity of gut microbiota influences the anti-tumour effect of the RCom, we supplemented the RCom to three cohorts of SPF mice with different baseline microbiota for each of the tumour models (Extended Data Fig. 9a). Only a small proportion (~30%) of baseline bacterial taxa were shared by all the three cohorts (Extended Data Fig. 9b). We found that despite the large variety of the baseline microbiota, RCom supplementation in combination with anti-PD-1 led to reduced tumour size and weight of both LLC and B16-F10 in all the three cohorts (Fig. 4k,l and Extended Data Fig. 9c-f). Accordingly, RCom supplementation induced functional CD8$^+$ T cells in the tumour and spleen of mice from all the three cohorts (Extended Data Fig. 9g). Therefore, enhancement of anti-tumour immunity and anti-PD-1 efficacy by the RCom was not influenced by a large variety of the baseline microbiota.

RCom supplementation circumvents resistance to anti-PD-1

We investigated whether supplementation of the RCom could overcome resistance to PD-1 blockade in mouse models. FMT using faecal samples from non-responder patients has been shown to convey resistance to PD-1 blockade in mice[13]. Thus, we reconstituted the gut microbiota in antibiotic (ATB)-pretreated SPF mice through FMT using donor samples from non-responder patients with advanced NSCLC amenable to anti-PD-1 (Supplementary Table 15). We first evaluated the combined efficacy of prophylactic RCom supplementation and anti-PD-1 therapy in LLC-bearing mice with humanized gut microbiota (Extended Data Fig. 10a–c). FMT from the non-responder patients conferred resistance to anti-PD-1 (Fig. 5 and Extended Data Fig. 10), which is consistent with previously published results[13]. Supplementation of the RCom was found to restore the anti-tumour activity of anti-PD-1 (Extended Data Fig. 10d,e). Notably, the combination of RCom and anti-PD-1 was able to cause tumour regression in mice (Extended Data Fig. 10d,e). This therapeutic efficacy was accompanied by increased infiltration of CD8$^+$ T cells into tumours and promoted the cytotoxic function of CD8$^+$ T cells (Extended Data Fig. 10f,g).

Finally, we tested RCom administration in a therapeutic setting. SPF mice with FMT from non-responder patients were orally supplemented with the RCom after LLC tumour inoculation (Fig. 5a). The three non-responder donors showed a large degree of heterogeneity in their faecal microbiota, with only 20% of bacterial taxa shared by all of them (Fig. 5b and Extended Data Fig. 10b). The engraftment of RCom members in mice with FMT was not assessed. However, combined treatment of the RCom and anti-PD-1 led to a significant decrease in tumour growth in mice with FMT from all the non-responder donors (Fig. 5c,d). Therefore, therapeutic supplementation of RCom circumvented the anti-PD-1 resistance in mice conferred by FMT from non-responder patients.

Discussion

Administration of a defined microbial consortium of cultivated species provides a promising approach of modulating the gut microbiota to improve the efficacy of ICIs, which integrates the benefits of the ecological balance of FMT with the scalability and practicality of probiotics. In this study, we designed and built a 15-member bacterial consortium, RCom, from the faecal microbiota of anti-PD-1-responding patients. Oral administration of the RCom was found to improve the anti-tumour activity of anti-PD-1 in multiple tumour models and in both prophylactic and therapeutic settings. Moreover, therapeutic supplementation of the RCom circumvented the anti-PD-1 resistance in mice conferred by FMT from non-responder patients. Although several microbial consortia have been developed for improving ICI immunotherapy, the available data from clinic studies indicate limited levels of engraftment depending on the native microbiota of patients[27,30]. Indeed, the baseline gut microbiota also influences the success of dietary interventions, FMT and probiotic engraftment[46,47,53]. However, interindividual microbial heterogeneity has not been taken into account adequately in previous designs of these microbiota-targeting interventions[19]. We showed that despite a large variety of the mouse native microbiota or the transplanted faecal microbiota from non-responder patients, enhancement of anti-PD-1 efficacy by the RCom was not influenced. Our results suggest that administration of the RCom is capable of reproducibly modulating the microbiota clinically to augment the effectiveness of ICI treatment.

Synthetic microbial consortia have been designed and assembled for modulating host-associated microbiota[21,54,55]. However, the intracommunity interactions have rarely been incorporated into the design. Here, through GEM-based prediction in silico and experimental characterization in vitro and in vivo, the RCom was designed and validated as a relatively cooperative community. The Firmicutes species showed metabolic dependencies on the Bacteroidetes species within the community, and supplementation of the latter species was required for enhancing the engraftment of the former species in mice. The intracommunity beneficial interactions probably enabled successful engraftment of the RCom, especially the involved Firmicutes species, in the presence of a large variety of baseline microbiota (Extended Data Fig. 10h). We showed the functional redundancy and stability of the RCom-supplemented gut microbiota. Supplementation of all the RCom members to mice robustly increased bacterial production of butyrate and acetate and degradation of adenine ribonucleotide to produce inosine, hypoxanthine and IMP. Butyrate and inosine have been shown to be capable of modulating immune function (a detailed discussion follows in the next paragragh). The RCom Firmicutes species could make an important contribution to production of these metabolites. More research is required to better understand the role of individual RCom members in supporting community functions.

Several mechanisms by which the commensal bacteria shape anti-tumour immunity have been reported[29]. Our results indicated that enhancement of anti-PD-1-induced anti-tumour immunity by the RCom

https://doi.org/10.1038/s41564-026-02279-6

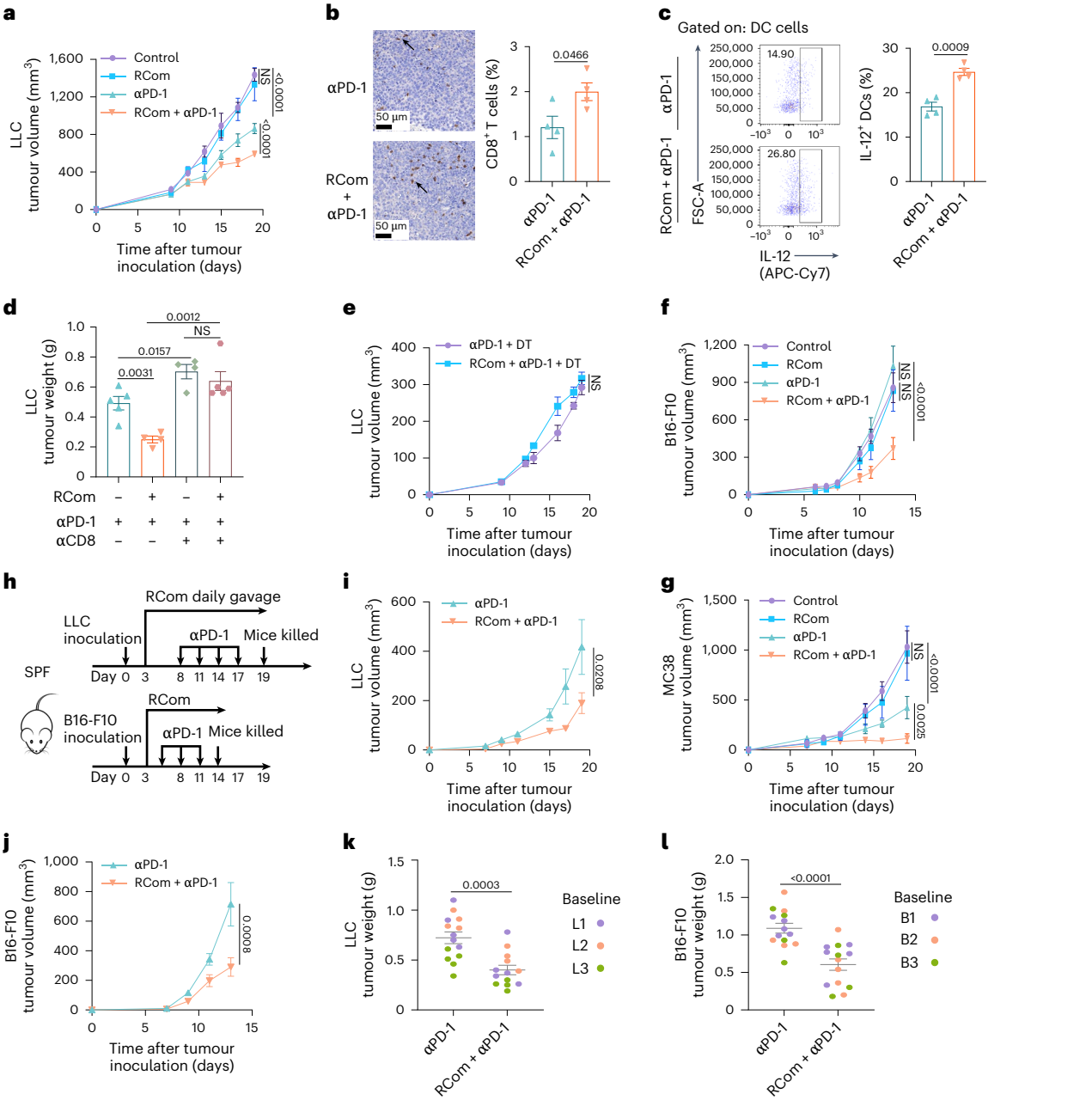

Fig. 4 | RCom administration enhances anti-PD-1 efficacy in tumour mouse models with a variety of baseline microbiota. a, SPF C57BL/6 mice were s.c. injected with tumour cells, and an anti-PD-1 antibody was injected i.p. Supplementation of RCom or PBS daily by oral gavage started 1 week before tumour inoculation. The tumour growth curve of LLC is shown. Control, RCom, $n = 5$ mice per group; αPD-1, RCom + αPD-1, $n = 4$ mice per group. **b**, Immunohistochemistry and quantification of $CD8^+$ T cells within LLC tumours from RCom- and PBS-fed mice with anti-PD-1 treatment. The arrows indicate $CD8^+$ T cells. $n = 4$ mice per group. **c**, Representative flow cytometry plots and quantification of $IL\text{-}12^+$ of DCs within LLC tumours from anti-PD-1-treated mice supplemented with RCom or PBS. $n = 4$ mice per group. **d**, Effect of $CD8^+$ T cell depletion on tumour weight at termination in anti-PD-1-treated mice fed with RCom or PBS. An anti-CD8 antibody was injected i.p. for the depletion. RCom + αPD-1, αPD-1 + αCD8, $n = 4$ mice per group; αPD-1, RCom + αPD-1 + αCD8, $n = 5$ mice per group. **e**, Tumour growth of LLC in DC-depleted and anti-PD-1-treated mice supplemented with RCom or PBS. DCs were depleted by intraperitoneal injection of diphtheria toxin (DT). $n = 5$ mice per group. **f**,**g**, Tumour growth of B16-F10 (**f**) ($n = 4$ mice per group) and MC38 (**g**) (RCom, αPD-1 $n = 4$ mice per group; control, RCom + αPD-1, $n = 5$ mice per group) in anti-PD-1-treated mice supplemented with RCom or PBS in a prophylactic setting. **h**, Schematic of the therapeutic experimental set-up. SPF C57BL/6 mice were s.c. injected with LLC or B16-F10 tumours followed by intraperitoneal injections of anti-PD-1. Supplementation of the RCom or PBS daily by oral gavage started 3 days after tumour inoculation. **i**,**j**, LLC (**i**) ($n = 5$ mice per group) and B16-F10 (**j**) (αPD-1, $n = 4$; RCom + αPD-1, $n = 5$) tumour growth in anti-PD-1-treated mice therapeutically supplemented with RCom or PBS. **k**,**l**, Three cohorts of SPF mice with different baseline gut microbiota were daily supplemented with RCom or PBS and injected s.c. with LLC or B16-F10 tumours followed by anti-PD-1 treatment. The weight of the LLC tumour (**k**) (L1: $n = 4$ mice per group; L2: $n = 5$ mice per group; L3: αPD-1, $n = 5$; RCom + αPD-1, $n = 4$) and B16-F10 (**l**) (B1: $n = 5$ mice per group; B2: $n = 5$ mice per group; B3: $n = 4$ mice per group) at termination was measured. Data are mean values and s.e.m. Two-way ANOVA (**a**, **e**–**g**, **i**, **j**) or two-tailed unpaired *t*-test (**b**–**d**, **k**, **l**). NS, not significant.

https://doi.org/10.1038/s41564-026-02279-6

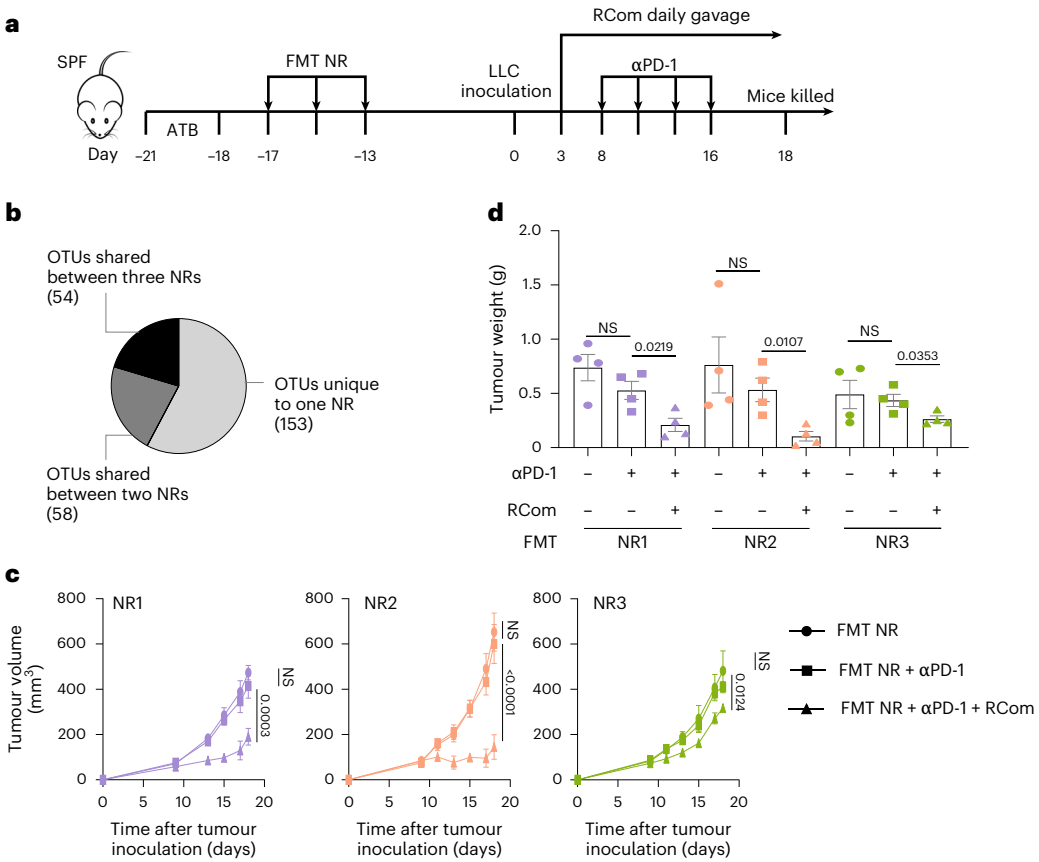

Fig. 5 | Therapeutic RCom supplementation circumvents the anti-PD-1 resistance in mice conferred by FMT from non-responder patients. a, Schematic of the experimental set-up. FMTs of faecal samples from three non-responder (NR) patients with NSCLC were individually performed in SPF C57BL/6 mice pretreated with ATB for 3 days. LLC tumours were inoculated 13 days later, and daily gavage of the RCom was performed in combination with intraperitoneal injections of anti-PD-1. **b**, Shared and unique OTUs between the three FMT donors. **c**,**d**, LLC tumour growth curve (**c**) and tumour weight at termination (**d**) in RCom- and anti-PD-1-treated mice with FMT from the three NR donors. Data are mean and s.e.m. $n = 4$ mice per group (**c** and **d**). Two-way ANOVA (**c**) or two-tailed unpaired t-test (**d**). NS, not significant.

is dependent on CD8$^+$ T cells. Supplementation of the RCom increased intratumoral infiltration and cytotoxic activity of CD8$^+$ T cells, and this positive effect was strongly diminished in DC-depleted mice. These results suggest that the RCom could improve anti-tumour responses of CD8$^+$ T cells by triggering DC activation (Extended Data Fig. 10h). Upregulation of IL-12 on DCs was observed for RCom-supplemented mice, supporting an involvement of IL-12 in the induction of CD8$^+$ T cell responses[56,57]. Bacterial metabolites produced by the RCom-supplemented gut microbiota, including butyrate and inosine, could play a crucial role in promoting anti-tumour immunity. Indeed, butyrate has been shown to boost CD8$^+$ T cell anti-tumour response in an IL-12-dependent manner[52]. Inosine can promote DC-dependent activation of anti-tumour T cells[45]. In addition, butyrate and inosine can serve as an energy or carbon source for CD8$^+$ T cells[58,59]. Further studies are required to elucidate the mechanisms through which the RCom-supplemented gut microbiota modulates the local immune responses and anti-tumour immunity in the presence of anti-PD-1.

High abundance of the RCom is associated with improved clinic outcomes in the cohort of this study and independent ICI-treated cancer cohorts[13,40,41]. A number of the RCom species are consistently enriched in ICI-responsive patients with cancer. Several of them (for example, *D. formicigenerans*) are associated with reduced risk of severe irAEs[33]. None of the RCom members have prominent virulence factors, toxins or multidrug-resistance genes. Thus, administration of the RCom could be safe and tolerable clinically. Altogether, our developed consortium, RCom, holds promise to improve the success rate of ICI therapy in patients with cancer.

Methods

Human study participants

Faecal samples were collected from patients with informed consent at Shanghai Chest Hospital affiliated to Shanghai Jiao Tong University between October 2016 and July 2023. These patients had stage IIIB or IV NSCLC with squamous or non-squamous histology and had documented recurrence or progression after at least one previous line of treatment (Supplementary Table 1). Patients with known epidermal growth factor receptor mutations who previously received tyrosine kinase inhibitors were also included. Patients did not receive financial participant compensation. A total of 59 patients were treated with PD-1 monoclonal antibody every 2 or 3 weeks. Tumour response was assessed using the Response Evaluation Criteria in Solid Tumours (RECIST), version 1.1 (ref. 12). Responders were defined by complete or partial response, or stable disease for 6 months or more, and non-responders were defined by stable disease lasting less than 6 months or progressive disease[14]. Faeces were collected before the anti-PD-1 treatment according to the study protocol approved by the Ethics Committee of Shanghai Chest Hospital (approval number KS23014-A). Samples were suspended in 20% glycerol in PBS, immediately frozen and stored at −80 °C.

Bacterial strains

To isolate bacterial strains enriched in responder patients, faecal contents from four patients (Supplementary Table 6) were filtered through a 200-μm cell strainer, serially diluted with PBS and seeded onto agar plates with 14 different growth media

(Supplementary Table 7). The media used for growing diverse microorganisms included brain–heart infusion (BHI), yeast extract–cellobiose–haemin–cysteine-supplemented BHI (LYHBHI), yeast extract–casein hydrolysate–fatty acids (YCFA), gut microbiota medium, chopped meat medium, Gifu anaerobic medium, reinforced *Clostridium* media and fastidious anaerobe[60]. Plates were incubated under anaerobic conditions (80% N_2, 10% H_2, 10% CO_2) in an anaerobic chamber (Thermo Fisher) at 37 °C for 2-4 days. Individual colonies were picked, and the 16S rRNA gene was PCR amplified with universal primers (27F: 5′-AGAGTTTGATCMTGGCTCAG-3′; 1492R: 5′-GGTTACCTTGTTACGACTT-3′) and sequenced. The resulting sequences were compared with those in the 16S ribosomal RNA sequence (Bacteria and Archaea) database at the National Center for Biotechnology Information (NCBI) to determine closely related species or strains. The obtained 192 bacterial isolates were assigned to 104 strains belonging to 42 distinct species. Among them, 10 strains were completely sequenced and included in the synthetic community RCom based on a design process illustrated in Extended Data Fig. 1a. Five other strains in the community (*A. finegoldii* DSM 17242, *A. inops* DSM 28863, *D. formicigenerans* DSM 3992, *Dorea longicatena* DSM 13814 and *Lachnospira eligens* ATCC 27750) were obtained from public repositories. These strains were originally isolated from human samples, and their genomic sequences were obtained from GenBank. For comparison, 13 bacterial strains were isolated from faecal samples from non-responder patients using the same method as described above.

Mice

All mouse experiments were conducted in accordance with protocols approved by the Institutional Animal Care and Use Committee of Shanghai Jiao Tong University (IACUC number: A2025207). Mice were randomly assigned to different experimental groups, and no animals were excluded from the analyses. SPF female C57BL/6 mice (6–8 weeks old) were obtained from two different commercial suppliers including Charles River and Shanghai Lingchang Biotechnology. For the study of batch effects, mice were obtained from the latter supplier in three different shipment batches at least 1 month apart. SPF female BALB/c mice and B-Cd11c-EGFP-DTR-Luc mice (6–8 weeks old) were purchased from Shanghai Lingchang Biotechnology and Biocytogen, respectively. All mice were kept at a room temperature of 24 ± 1 °C, room humidity of 30–70% and a 12–12-h light–dark cycle (7:00 a.m.–7:00 p.m.). After acclimatizing to a standard diet rich in fibre (Purina LabDiet 5001) and housing environment for 1 week, mice were randomly separated into experimental groups.

Metagenomic analysis of faecal microbiota from patients

Frozen faecal samples were thawed, and DNA was extracted using the SPINeasy DNA Kit for faeces (MP Biomedicals) according to the manufacturer's instructions. DNA concentration was determined spectrophotometrically using a NanoDrop 2000 (Thermo Fisher). Whole-genome shotgun libraries were prepared using the VAHTS Universal DNA Library Prep Kit for Illumina (Vazyme), and 2 × 150 bp paired-end sequencing was performed on an Illumina NovoSeq 6000. The sequencing reads were adaptor removed, trimmed for quality and filtered for host contamination using KneadData v.0.61 (http://huttenhower.sph.harvard.edu/kneaddata) with the human reference databases (GRCh37). Taxonomical annotation of metagenomic species was performed using Kraken 2 v.2.0.9, which is based on exact alignment of short stretches of genes (*k*-mers), with a standard database including NCBI RefSeq (>30,000 genomes). The relative abundances of all the annotated species were estimated and calibrated using Bracken 2 that computes the abundance of species in DNA sequences from a metagenomic sample based on Bayesian statistical modelling. The LEfSe method was used to compare the abundance of all bacterial species according to the response of patients to anti-PD-1 treatment. The species with differential abundance between responders and non-responders ($P < 0.05$) were used as input for the LDA to calculate an effect size (LDA score).

Bacterial genome sequencing

The genomic DNA of the 10 isolated strains of the RCom was extracted using the QIAamp DNA Mini Kit (Qiagen). The genome sequences were determined by using a whole-genome shotgun method as described above. All sequencing reads were trimmed and assessed for quality control by the Trimmomatic (v.0.32) software. Trimmed reads were assembled using SPAdes v.3.10.1 with default parameters, and the assembly quality was checked using QUAST v.4.5. The bacterial genomes were searched for putative toxins and virulence factors according to the Comprehensive Antibiotic Resistance Database (CARD, https://card.mcmaster.ca) and the bacterial Virulence Factor Database (VFDB, https://www.mgc.ac.cn/VFs) at a threshold of 70% of identity and 70% of gene length coverage.

Metabolic interaction simulations

GEMs for individual bacterial species were downloaded from AGORA (assembly of gut organisms through reconstruction and analysis) (https://www.vmh.life/files/reconstructions/AGORA). These GEMs were used as input for SMETANA v.1.0 to compute the MRO and SMETANA score of synthetic communities as reported previously[38]. MRO was used to assess metabolic competition by measuring the overlap between the minimal nutritional requirements of all member species on the basis of their genomes. The SMETANA score provided a measure of all possible interspecies dependencies under a given nutritional condition. Simulations were carried out on the basis of a minimal medium[38].

In vitro growth experiments

The chemically defined (CD) medium (Supplementary Table 8) used for bacterial cultivation was modified from a YCFA-defined medium[61]. To test the substrate-utilizing capability of individual species, bacterial cells were cultured in 96-well flat-bottom plates with 200 µl per well of the medium containing 2 g l^{-1} of D-glucose, D-fructose, D-xylose, *N*-acetylglucosamine, mannose, cellobiose, fructo-oligosaccharide, xylan, galactan, arabinoxylan, inulin, glycogen, starch or glucomannan. After 72 h of anaerobic cultivation at 37 °C, optical density at 600 nm (OD_{600}) was measured and normalized to the maximum values within each species and for the same substrate[62].

For community growth experiments, individual bacterial species were precultured on LYHBHI or YCFA medium overnight, washed twice with PBS and resuspended in the CD medium to OD_{600} of ~0.2. From the cell suspensions of 15 species, 50 µl each was pooled, and 100 µl of the mixture was used to inoculate 1.9 ml of fresh CD medium. In addition to equal ratio, two other inoculation ratios were tested, which were directly and inversely, respectively, proportional to the final relative abundances of individual species after 48 h of growth from an equally mixed inoculum (Supplementary Table 10). The community was cultured anaerobically at 37 °C for 48 h. Bacterial genomic DNA was extracted using the QIAamp DNA Mini Kit (Qiagen), and the abundance of each species was determined by qPCR.

Characterization of bacterial species interactions

To characterize pairwise interactions in the RCom, each species was precultured on LYHBHI or YCFA medium overnight, washed twice with PBS and resuspended in CD medium to OD_{600} of ~0.2. From the cell suspensions of two species, 50 µl each was pooled, and the mixture was passed into 10-ml sterile tubes containing 1.9 ml of fresh CD medium. The cultures of single species were used as controls. The co-cultures and monocultures were grown anaerobically at 37 °C for 48 h, and the abundance of each species was quantified by qPCR. The growth of the species in co-culture was compared with that in monoculture. The effect of one species on the other was classified into positive, negative or neutral depending on the growth change of the other species. The

identified positive interactions corresponded to at least 100% increase in the growth, and they were classified as mutualism and commensalism based on the reciprocal effects.

To detect metabolic cross-feeding between Bacteroidetes and Firmicutes species in the RCom, 5 Bacteroidetes species were cultivated in 5 ml of CD medium lacking amino acids (CD-AA). The medium contained 1 g l^{-1} of uniformly ^{13}C-labelled glucose ([U-^{13}C]glucose) or unlabelled glucose. After incubation for 12 h (a duration that ensured that the glucose in the medium had been just exhausted), the culture medium was collected by centrifugation at 3,500 × *g* for 5 min at room temperature, followed by filtration with a 0.22-µm syringe filter. Then, 4 ml of the filtered medium and 16 ml of fresh CD-AA medium containing 2 g l^{-1} glucose were pooled. The medium was used to resuspend PBS-washed cells of 10 Firmicutes species to OD_{600} ~0.005 each, and the community was grown anaerobically at 37 °C for 48 h. At the indicated time points, the culture supernatant was collected by centrifugation and used for metabolomic analysis. The cell pellets were used for proteomic analysis.

qPCR analysis

The bacterial species-specific primers (Supplementary Table 9) were designed based on randomly selected species-specific genes by comparing the primer and target gene sequences against sequences in public databases. The primers were synthesized by Beijing Tsingke Biotech. The melting curve analysis for qPCR of mouse faecal DNA showed a single peak at ~83 °C for each species. The specificity of each primer set was further validated by qPCR of a non-target template composed of bacterial genomic DNA from the other 14 species in the RCom and 8 common species in the human gut microbiota. The qPCR analyses were performed using Hieff qPCR SYBR green master mix (Yeasen) on the CFX96 thermal cycler (Bio-Rad). The amount of the bacterial species was quantified by plotting a standard curve of varying concentrations of its genomic DNA.

16S rRNA gene amplicon sequencing

The V3–V4 region of the bacterial 16S rRNA gene was amplified using the following primers: forward, 5′-CCTACGGRRBGCASCAGKVRVGAAT-3′; reverse, 5′-GGACTACNVGGGTWTCTAATCC-3′. The amplicons were attached with dual indices and Illumina sequencing adaptors by PCR. After purification and quantification of the PCR products, sequencing was carried out on a MiSeq platform (Illumina) using 2 × 250 bp paired-end sequencing. The sequences were processed using QIIME2 v.2019.4. Filtered high-quality reads were clustered into operational taxonomic units (OTUs) with a 97% pairwise-identity cut-off. Taxonomic annotation was performed on the basis of the SILVA r132 database.

MAG assembly and functional annotation

DNA was extracted from mouse caecal samples and sequenced following the protocol used for human samples. Metagenomes of caecal microbiota were co-assembled within groups using MEGAHIT (v.1.2.9) with default parameters. The contigs longer than 1,000 kb were binned into MAGs using three different tools: MetaBAT2 (v.2.12.1), MaxBin (v.2.2.4) and CONCOCT (v.0.4.0), which were then integrated with MetaWRAP (v.0.8). MAG completion and contamination were assessed using CheckM (v.1.1.2). MAGs were conservatively kept in the local MAG database if they were >50% complete and <10% contaminated. De-replication of MAGs at 99% identity was carried out using dRep (v.2.6.2). The MAGs were taxonomically classified with the NCBI RefSeq. Functional annotation of the MAGs was performed using a recently reported workflow[63]. Briefly, the level of completeness for a given Kyoto Encyclopedia of Genes and Genomes module in the genomes was determined using the program 'anvi-estimate-metabolism' in anvi'o (v.7.1). The program 'anvi-compute-functional-enrichment' was then used to determine whether a given metabolic module was enriched in a group of genomes. The enrichment scores for metabolic modules within groups were computed by fitting a binomial generalized linear model to the occurrence of each complete metabolic module in each group.

Subcutaneous tumour models and bacterial supplementation

To prepare the bacterial communities for in vivo experiments, individual species were grown on LYHBHI or YCFA medium overnight and washed with PBS, and appropriate volumes of cell suspensions were mixed. The mixture (200 µl) containing about 4 × 10^8 colony-forming units (CFU) of each bacterial species was daily supplemented by oral gavage to SPF C57BL/6 mice. PBS was used as a control. A heat-killed bacterial mixture was obtained by heating at 99 °C for 1 h. After gavage of the indicated bacterial mixtures for 7 days, caecal contents were collected. DNA was extracted for qPCR analysis and metagenomic sequencing, and metabolites were extracted for metabolomic analysis.

LLC cells (catalogue number CRL-1642), B16-F10 melanoma cells (catalogue number CRL-6475) and MC38 colorectal adenocarcinoma cells (catalogue number AC337600) were obtained from ATCC. CMT-167 lung adenocarcinoma cells (catalogue number BFN60808932) bearing an oncogenic KRAS G12V mutation and ASB-XIV pulmonary squamous carcinoma cells (catalogue number BFN60904188) were purchased from Shanghai Bluefbio Biology Technology Development. Cells were cultured in RPMI 1640 (HyClone) or DMEM (HyClone) with 10% fetal bovine serum (FBS, SuperCulture) and 100 U ml^{-1} penicillin and streptomycin at 37 °C in the presence of 5% CO_2. SPF C57BL/6 mice were subcutaneously (s.c.) injected with 4 × 10^5 LLC cells, 2 × 10^5 B16-F10 cells, 3 × 10^5 MC38 cells or 2 × 10^6 CMT-167 cells on day 0. BALB/c mice were s.c. injected with 1.5 × 10^6 ASB-XIV cells. For the bacterial supplementation groups, the bacterial mixture was orally given to mice starting 1 week before tumour inoculation (prophylactic approach) or 3 days after tumour inoculation (therapeutic approach). Daily supplementation of the bacterial cocktail continued until the end of the experiment. Mice were intraperitoneally (i.p.) injected with 200 µg PD-1 monoclonal antibody (clone RMP1-14, BioXCell) on days 8, 11, 14 and 17 after LLC or MC38 inoculation or on days 5, 8 and 11 after B16-F10 or CMT-167 inoculation. Anti-PD-1 (100 µg) was given once on day 8 after ASB-XIV inoculation. For depletion of $CD8^+$ T cells, administration of 200 µg anti-CD8 monoclonal antibody (clone 2.43, BioXCell) weekly by intraperitoneal injection started 2 days before LLC inoculation. For DC depletion, diphtheria toxin (50 ng per g of body weight, Listbio) was i.p. injected into B-Cd11c-EGFP-DTR-Luc mice on days −9 and −8. Tumour size was measured 3–4 times per week and volume was determined as length × $width^2$ × 0.5. According to animal ethics, mice were euthanized when tumour volume reached 1,500 mm^3. Otherwise, mice were euthanized at the indicated time points, and tumour weight was measured.

For FMT experiments, frozen faecal materials from patients with NSCLC amenable to anti-PD-1 were thawed for use. SPF C57BL/6 mice were treated with ampicillin (1 g l^{-1}), streptomycin sulfate (5 g l^{-1}) and colistin sulfate (1 g l^{-1}) for 3 days via drinking water. After a 1-day antibiotic washout, 200 µl of the faecal suspension was transferred by oral gavage into each antibiotic-pretreated mouse on days −17, −15 and −13. The RCom was administered daily from day −7 for the prophylactic approach or from day 3 for the therapeutic approach. LLC cells were injected s.c. on day 0, and anti-PD-1 injection and tumour measurement were performed as described above.

Histological analysis

Tissue sections (5 µm) were prepared from paraffin-embedded tumour samples. The slides were heated in antigen retrieval solution (Servicebo). Endogenous peroxidases were blocked with 3% H_2O_2, and unspecific antibody binding was blocked with 3% BSA in PBS. A primary anti-CD8 antibody (Servicebo) was applied at 4 °C overnight. The slides were then incubated with the secondary antibody (HRP-labelled goat anti-mouse IgG, Servicebo) for 50 min at room temperature. After DAB staining, the slides were counterstained with haematoxylin, dehydrated and fixed. Images were captured using a Pannoramic 250

FLASH microscope (3DHISTECH). Quantification of positive cells was performed using ImageJ software (v.1.52a).

Flow cytometry analysis

Colonic lamina propria cells were isolated as described previously[64]. Briefly, colons were opened longitudinally, and adipose tissue and lymph nodes were removed using forceps. After washing with PBS to remove luminal contents, the samples were incubated in PBS containing 1 mM dithiothreitol, 30 mM EDTA and 10 mM HEPES for 10 min and then in PBS containing 30 mM EDTA and 10 mM HEPES for 10 min at 37 °C in a shaking water bath to remove the mucous layer and epithelial cells. The remaining lamina propria layer was cut into small pieces and incubated in 4 ml of RPMI 1640 medium containing 10% FBS, 0.5 mg ml^{-1} type VIII collagenase (Sigma-Aldrich) and 0.15 mg ml^{-1} DNase I (Sigma-Aldrich) for 55 min at 37 °C in a shaking water bath. The digested tissues were homogenized by vigorous shaking and then filtered through a 70-µm cell strainer.

For analysis of intratumoural CD8$^+$ T cells and DCs, tumours were cut into small pieces and digested using a tumour dissociation kit (Miltenyi Biotec) as per the manufacturer's instructions. The resulting cell suspension was passed through a 70-µm cell strainer. After centrifugation, the pellets were incubated in ACK lysis buffer (eBioscience) for 5 min at room temperature to remove red blood cells, and RPMI 1640 medium was added. Pelleted cells were resuspended in PBS containing 2% FBS for further staining. The spleens were homogenized and filtered through a 70-µm cell strainer followed by removal of red blood cells.

For surface staining, the following antibodies were used: anti-CD45 (AF700, Invitrogen), CD3 (BV711, Biolegend), CD4 (BV786, BD Biosciences), CD8α (BV650, Biolegend), TCRβ (PerCP-Cy5.5, Biolegend), CD44 (BV785, Biolegend), CD62L (APC-R700, BD Biosciences), NK1.1 (FITC, eBioscience), B220 (PerCP-Cy5.5, BD Biosciences), CXCR3 (BV421, Biolegend), I-A/I-E (Percp-cy5.5, BD Biosciences), CD86 (PE, BD Biosciences), CD80 (APC, BD Biosciences), CD103 (FITC, eBioscience), CD11c (BV785, Biolegend), CD11b (AF700, Biolegend), H-2Kb (PE/Cy7, Biolegend), Ly6G (BV786, BD Biosciences), Siglec F (BV421, BD Biosciences) and CD64 (BV711, Biolegend). For cytokine detection, single-cell suspensions were stimulated with 100 ng ml^{-1} PMA (Sigma-Aldrich) and 1 µg ml^{-1} ionomycin (Sigma-Aldrich) in the presence of GolgiStop (BD Biosciences) at 37 °C for 4 h. After surface staining, cells were permeabilized using a Cytofix/Cytoperm fixation and permeabilization kit (BD Biosciences). The following antibodies were used for detection of cytokines and proteins: IFNγ (BV421, BD Biosciences), GzmB (PE, Invitrogen), TNF (PE/Cy7, eBioscience), CD107a (FITC, BD Biosciences), IL-2 (BV605, Biolegend), IL-12 (APC/Cy7, Biolegend), Foxp3 (APC, Invitrogen) and Ki67 (PerCP-Cy5.5, BD Biosciences). The flow cytometry gating strategies are described in Supplementary Fig. 6. Comprehensive details for all antibodies have been compiled in Supplementary Table 16. All data were collected on a BD LSRFortessa X-20 (BD Biosciences) instrument and analysed with FlowJo software (v.10.0, TreeStar).

Proteomic analysis

Proteomic samples were prepared as described previously with minor modifications[65]. Briefly, approximately 1×10^9 bacterial cells were resuspended in 500 µl of lysis buffer containing 6 M guanidinium chloride, 5 mM Tris(2-carboxyethyl)phosphine (TCEP) and 100 mM Tris-HCl (pH 7.4). Cells were lysed by sonication on ice, and the supernatant was collected after centrifugation at 20,000 × *g* for 20 min at 4 °C. Protein was precipitated by methanol and chloroform. The dried protein pellet was resuspended in 8 M urea and alkylated with 50 mM chloroacetamide and 10 mM TCEP in 50 mM ammonium bicarbonate for 30 min at 30 °C. TCEP was used to quench the excessive alkylating reagents. The protein mixture was diluted with 100 mM ammonium bicarbonate to ensure that the urea concentration was less than 1 M and then digested with 10 ng µl^{-1} trypsin (mass spectrometry grade, Promega) at 37 °C for 2 h. Proteins were further digested with 20 ng µl^{-1} trypsin at 37 °C overnight. Samples were desalted using SepPak cartridges (Waters), vacuum dried and resuspended in 0.1% formic acid.

Samples containing 1 µg of peptides were analysed by an ultrahigh-performance liquid chromatograph (EASY-nLC 1200, Thermo Fisher) coupled to a quadrupole-orbitrap mass spectrometer (Q-Exactive HF-X, Thermo Fisher). Peptides were separated with a C18 reverse-phase analytical column (25 cm by 75 µm internal diameter, 1.9 µm particle size; Shanghai Easymass). The column was maintained at 55 °C with a flow rate of 300 nl min^{-1}. Solvent A was water with 0.1% formic acid, and solvent B was 80% acetonitrile with 0.1% formic acid. The gradient of B was as follows: 0 min, 3%; 3 min, 8%; 105 min, 28%; 112 min, 45%; 113 min, 100%; and 120 min, 100%. The parameters of the mass spectrometer were set as follows: ion spray voltage, 2 kV, and capillary temperature, 350 °C. Full-scan mass spectra with mass range 350-1,500 *m*/*z* were acquired with a resolution of 60,000. The filling time was set at a maximum of 50 ms with a limitation of 3×10^6 ions. The most intense ions (up to 20) from the full-scan MS were selected for MS/MS. A normalized collision energy of 30% was used, and the fragmentation was performed after a filling time of 25 ms for each precursor ion. MS/MS spectra were acquired with a resolution of 15,000.

Data were analysed using MetaProSIP, Konstanz Information Miner (KNIME, v3.6.2) and OpenMS as described previously[44]. Briefly, LC–MS raw data were converted to mzML format using ProteoWizard, which were further processed by KNIME to identify unlabelled peptides and their ^{13}C-labelled isoforms. Data were searched against the combined reference proteomes for the 10 Firmicutes species in the RCom. The target-decoy strategy was used to construct a second database of reverse sequences for estimating the peptide false discovery rate. The unlabelled peptides were identified with OpenMS MSGFPlusAdapter. MetaProSIP was then used to detect the labelled peptides, extract the related peaks and calculate the labelling ratio. Proteins were inferred from the identified peptides by requiring a minimum of two unique peptides per protein. Peptides that were identified in only two out of the three replicates and had a high coefficient of variation (>25%) were filtered out. The detected species-specific peptides are shown in Supplementary Table 11.

Metabolomic analysis

Metabolite extraction from mouse caecal contents was performed as described previously[66]. In brief, ~50 mg frozen caecal contents were resuspended in −20 °C 80% methanol and homogenized with 1-mm zirconia–silica beads (Biospec) in a tissue homogenizer (Bertin). After incubation at −20 °C for 20 min, the samples were centrifuged at 20,000 × *g* for 10 min at 4 °C, and the supernatant was collected for LC–MS analysis. Quality control samples were prepared by pooling aliquots of all caecal samples and mixing thoroughly.

Metabolites were analysed using an ultrahigh-performance liquid chromatograph (UltiMate 3000, Thermo Fisher) coupled to a quadrupole-orbitrap mass spectrometer (Q-Exactive, Thermo Fisher). To increase the coverage of metabolomic profiling, two different LC procedures were carried out[67]. Polar metabolites were separated with a Luna NH2 column (100 mm × 2 mm internal diameter, 3 µm particle size; Phenomenex). The injection volume was 3 µl. Mobile phase A was 20 mM ammonium acetate (pH 9.0) and B was acetonitrile. The column was maintained at 15 °C with a solvent flow rate of 0.3 ml min^{-1}, and the gradient of B was as follows: 0 min, 85%; 10 min, 45%; 15 min, 2%; 18 min, 2%; 18.1 min, 85%; and 25 min, 85%. The mass spectrometer was run in electrospray ionization negative (ESI$^-$) mode. Nonpolar metabolites were separated by reverse-phase chromatography using an XSelect HSS T3 column (100 mm × 3 mm, 2.5 µm; Waters). The injection volume was 10 µl. Mobile phase A was 0.1% formic acid in water and B was 0.1% formic acid in methanol. The column was maintained at 40 °C with a solvent flow rate of 0.4 ml min^{-1}, and the gradient of B was as follows: 0 min, 0%; 10 min, 50%; 14 min, 98%; 16 min, 98%; 16.1 min, 0%; and 18 min,

0%. The mass spectrometer was operated in electrospray ionization positive (ESI^+) mode. The parameters of the mass spectrometer were set as follows: ion spray voltage, +3.5 kV/−3.0 kV; capillary temperature, 320 °C; probe heater temperature, 350 °C; and sheath and auxiliary gas, 35 and 10 arb. units, respectively. Mass spectra were acquired using full scan over 70–1,000 m/z at 70,000 resolution. LC–MS data processing was performed as described previously[43]. Briefly, data were processed with Compound Discoverer v.3.3 (Thermo Fisher) followed by signal drift correction and quality checks using quality control samples to generate a data matrix consisting of retention time, m/z value and peak intensity. The accurate mass and acquired MS/MS spectra were used for metabolite identification by matching with in-house spectral libraries and online databases (mzCloud and Human Metabolome Database). Metabolite concentrations were determined by using a calibration curve generated with varying concentrations of the chemical standard.

Short-chain fatty acids were analysed using an ultrahigh-performance liquid chromatograph (ExionLC AD, SCIEX) coupled to a hybrid triple-quadrupole/linear ion trap mass spectrometer (QTRAP 5500, AB SCIEX). Based on a previous method with modifications[68], the caecal samples were mixed with an internal standard (4-methylvaleric acid) and derivatized with 3-nitrophenylhydrazine-hydrochloride (3NPH·HCl, Sigma-Aldrich) plus (*N*-(3-dimethylaminopropyl)-*N*′-ethylcarbodiimide hydrochloride (EDC·HCl, Sigma-Aldrich) at 37 °C for 1 h. After centrifugation, 1 µl of the sample was injected into the LC–MS instrument with a C18 column (100 mm × 2.1 mm internal diameter, 2.6 µm particle size; Phenomenex).

Statistical analyses

No statistical methods were used to predetermine sample sizes, but our sample sizes are similar to those reported in previous publications[26]. Data collection and analysis were not performed blind to the conditions of the experiments. Data distribution was assumed to be normal, but this was not formally tested. Statistical analyses were performed using GraphPad Prism (v.8.4.3) or SIMCA (for metabolomic analysis). The two-tailed unpaired Student's *t*-test (parametric) or two-tailed Mann–Whitney *U* test was used for all comparisons between two groups. Correlation of bacterial abundances from different inoculation ratios was assessed using two-tailed Pearson's test. Tumour growth curves were analysed by two-way ANOVA. The Kaplan–Meier method was used to estimate PFS or OS of patients, with the differences between the groups calculated with the log-rank test. HR was determined using stratified or simple Cox proportional hazard models. Differential abundances of bacterial species between patient groups across cohorts were analysed using MaAsLin2 linear models. Details including statistical tests, exact values and definition of *n* are provided in each figure legend.

Reporting summary

Further information on research design is available in the Nature Portfolio Reporting Summary linked to this article.

Data availability

Whole-genome shotgun sequencing data of human faecal samples (accession number PRJNA1195622), genomic sequences of the 10 isolated strains (PRJNA1312235), 16S rRNA (PRJNA1193840) and whole-genome shotgun sequencing data (PRJNA1196516) of mouse caecal samples have been deposited in the National Institutes of Health Sequence Read Archive. The proteomics data have been deposited in the PRIDE repository (PXD064618). Source data are provided with this paper.

Code availability

The code for metabolic interaction analysis and Cox regression analysis of survival generated in this study is available via GitHub at http://github.com/zhouhaiyan5555/RCom (ref. 69).

References

1. Ribas, A. & Wolchok, J. D. Cancer immunotherapy using checkpoint blockade. *Science* **359**, 1350–1355 (2018).
2. Robert, C. et al. Anti-programmed-death-receptor-1 treatment with pembrolizumab in ipilimumab-refractory advanced melanoma: a randomised dose-comparison cohort of a phase 1 trial. *Lancet* **384**, 1109–1117 (2014).
3. Motzer, R. J. et al. Nivolumab plus ipilimumab versus sunitinib in first-line treatment for advanced renal cell carcinoma: extended follow-up of efficacy and safety results from a randomised, controlled, phase 3 trial. *Lancet Oncol.* **20**, 1370–1385 (2019).
4. Reck, M. et al. Pembrolizumab versus chemotherapy for PD-L1-positive non-small-cell lung cancer. *N. Engl. J. Med.* **375**, 1823–1833 (2016).
5. Bagchi, S., Yuan, R. & Engleman, E. G. Immune checkpoint inhibitors for the treatment of cancer: clinical impact and mechanisms of response and resistance. *Annu. Rev. Pathol.* **16**, 223–249 (2021).
6. Topalian, S. L. et al. Five-year survival and correlates among patients with advanced melanoma, renal cell carcinoma, or non-small cell lung cancer treated with nivolumab. *JAMA Oncol.* **5**, 1411–1420 (2019).
7. Postow, M. A., Sidlow, R. & Hellmann, M. D. Immune-related adverse events associated with immune checkpoint blockade. *N. Engl. J. Med.* **378**, 158–168 (2018).
8. Vetizou, M. et al. Anticancer immunotherapy by CTLA-4 blockade relies on the gut microbiota. *Science* **350**, 1079–1084 (2015).
9. Sivan, A. et al. Commensal *Bifidobacterium* promotes antitumor immunity and facilitates anti-PD-L1 efficacy. *Science* **350**, 1084–1089 (2015).
10. Jin, Y. et al. The diversity of gut microbiome is associated with favorable responses to anti-programmed death 1 immunotherapy in Chinese patients with NSCLC. *J. Thorac. Oncol.* **14**, 1378–1389 (2019).
11. Derosa, L. et al. Negative association of antibiotics on clinical activity of immune checkpoint inhibitors in patients with advanced renal cell and non-small-cell lung cancer. *Ann. Oncol.* **29**, 1437–1444 (2018).
12. Pinato, D. J. et al. Association of prior antibiotic treatment with survival and response to immune checkpoint inhibitor therapy in patients with cancer. *JAMA Oncol.* **5**, 1774–1778 (2019).
13. Routy, B. et al. Gut microbiome influences efficacy of PD-1-based immunotherapy against epithelial tumors. *Science* **359**, 91–97 (2018).
14. Gopalakrishnan, V. et al. Gut microbiome modulates response to anti-PD-1 immunotherapy in melanoma patients. *Science* **359**, 97–103 (2018).
15. Matson, V. et al. The commensal microbiome is associated with anti-PD-1 efficacy in metastatic melanoma patients. *Science* **359**, 104–108 (2018).
16. Baruch, E. N. et al. Fecal microbiota transplant promotes response in immunotherapy-refractory melanoma patients. *Science* **371**, 602–609 (2020).
17. Davar, D. et al. Fecal microbiota transplant overcomes resistance to anti-PD-1 therapy in melanoma patients. *Science* **371**, 595–602 (2021).
18. Fernandes, M. R., Aggarwal, P., Costa, R. G. F., Cole, A. M. & Trinchieri, G. Targeting the gut microbiota for cancer therapy. *Nat. Rev. Cancer* **22**, 703–722 (2022).
19. Simpson, R. C., Shanahan, E. R., Scolyer, R. A. & Long, G. V. Towards modulating the gut microbiota to enhance the efficacy of immune-checkpoint inhibitors. *Nat. Rev. Clin. Oncol.* **20**, 697–715 (2023).

20. Lee, K. A., Shaw, H. M., Bataille, V., Nathan, P. & Spector, T. D. Role of the gut microbiome for cancer patients receiving immunotherapy: dietary and treatment implications. *Eur. J. Cancer* **138**, 149–155 (2020).
21. Vazquez-Castellanos, J. F., Biclot, A., Vrancken, G., Huys, G. R. & Raes, J. Design of synthetic microbial consortia for gut microbiota modulation. *Curr. Opin. Pharmacol.* **49**, 52–59 (2019).
22. Cheng, A. G. et al. Design, construction, and in vivo augmentation of a complex gut microbiome. *Cell* **185**, 3617–3636.e19 (2022).
23. Kelly, B. J., Kwon, J. H. & Woodworth, M. H. Escape velocity—the launch of microbiome therapies. *J. Infect. Dis.* **230**, 2–4 (2024).
24. Terveer, E. M. et al. Human transmission of blastocystis by fecal microbiota transplantation without development of gastrointestinal symptoms in recipients. *Clin. Infect. Dis.* **71**, 2630–2636 (2020).
25. Skelly, A. N., Sato, Y., Kearney, S. & Honda, K. Mining the microbiota for microbial and metabolite-based immunotherapies. *Nat. Rev. Immunol.* **19**, 305–323 (2019).
26. Tanoue, T. et al. A defined commensal consortium elicits CD8 T cells and anti-cancer immunity. *Nature* **565**, 600–605 (2019).
27. Spreafico, A. et al. First-in-class Microbial Ecosystem Therapeutic 4 (MET4) in combination with immune checkpoint inhibitors in patients with advanced solid tumors (MET4-IO Trial). *Ann. Oncol.* **34**, 520–530 (2023).
28. Oliva, I. G. et al. 607 MCGRAW trial: evaluation of the safety and efficacy of an oral microbiome intervention (SER-401) in combination with nivolumab in first line metastatic melanoma patients. *J. Immunother. Cancer* https://doi.org/10.1136/jitc-2022-SITC2022.0607 (2022).
29. Kang, X., Lau, H. C.-H. & Yu, J. Modulating gut microbiome in cancer immunotherapy: harnessing microbes to enhance treatment efficacy. *Cell Rep. Med.* **5**, 101478 (2024).
30. Glitza, I. C. et al. Randomized placebo-controlled, biomarker-stratified phase Ib microbiome modulation in melanoma: impact of antibiotic preconditioning on microbiome and immunity. *Cancer Discov.* **14**, 1161–1175 (2024).
31. Derosa, L. et al. Gut bacteria composition drives primary resistance to cancer immunotherapy in renal cell carcinoma patients. *Eur. Urol.* **78**, 195–206 (2020).
32. McCulloch, J. A. et al. Intestinal microbiota signatures of clinical response and immune-related adverse events in melanoma patients treated with anti-PD-1. *Nat. Med.* **28**, 545–556 (2022).
33. Andrews, M. C. et al. Gut microbiota signatures are associated with toxicity to combined CTLA-4 and PD-1 blockade. *Nat. Med.* **27**, 1432–1441 (2021).
34. Ramoneda, J., Jensen, T. B. N., Price, M. N., Casamayor, E. O. & Fierer, N. Taxonomic and environmental distribution of bacterial amino acid auxotrophies. *Nat. Commun.* **14**, 7608 (2023).
35. Gould, A. L. et al. Microbiome interactions shape host fitness. *Proc. Natl Acad. Sci. USA* **115**, E11951–E11960 (2018).
36. Van Der Lelie, D. et al. Rationally designed bacterial consortia to treat chronic immune-mediated colitis and restore intestinal homeostasis. *Nat. Commun.* **12**, 3015 (2021).
37. Magnusdottir, S. et al. Generation of genome-scale metabolic reconstructions for 773 members of the human gut microbiota. *Nat. Biotechnol.* **35**, 81–89 (2017).
38. Zelezniak, A. et al. Metabolic dependencies drive species co-occurrence in diverse microbial communities. *Proc. Natl Acad. Sci. USA* **112**, 6449–6454 (2015).
39. Kost, C., Patil, K. R., Friedman, J., Garcia, S. L. & Ralser, M. Metabolic exchanges are ubiquitous in natural microbial communities. *Nat. Microbiol.* **8**, 2244–2252 (2023).
40. Derosa, L. et al. Custom scoring based on ecological topology of gut microbiota associated with cancer immunotherapy outcome. *Cell* **187**, 3373–3389.e16 (2024).
41. Derosa, L. et al. Intestinal *Akkermansia muciniphila* predicts clinical response to PD-1 blockade in patients with advanced non-small-cell lung cancer. *Nat. Med.* **28**, 315–324 (2022).
42. Liu, R. et al. Gut microbial structural variation associates with immune checkpoint inhibitor response. *Nat. Commun.* **14**, 7421 (2023).
43. Zhang, H. et al. The cyanobacterial ornithine–ammonia cycle involves an arginine dihydrolase. *Nat. Chem. Biol.* **14**, 575–581 (2018).
44. Gabrielli, N. et al. Unravelling metabolic cross-feeding in a yeast–bacteria community using ^{13}C-based proteomics. *Mol. Syst. Biol.* **19**, e11501 (2023).
45. Mager, L. F. et al. Microbiome-derived inosine modulates response to checkpoint inhibitor immunotherapy. *Science* **369**, 1481–1489 (2020).
46. Zmora, N. et al. Personalized gut mucosal colonization resistance to empiric probiotics is associated with unique host and microbiome features. *Cell* **174**, 1388–1405.e21 (2018).
47. Zeevi, D. et al. Personalized nutrition by prediction of glycemic responses. *Cell* **163**, 1079–1094 (2015).
48. Liu, H. et al. Ecological dynamics of the gut microbiome in response to dietary fiber. *ISME J.* **16**, 2040–2055 (2022).
49. Randall, D. W. et al. Batch effect exerts a bigger influence on the rat urinary metabolome and gut microbiota than uraemia: a cautionary tale. *Microbiome* **7**, 127 (2019).
50. Buckel, W. Energy conservation in fermentations of anaerobic bacteria. *Front. Microbiol.* **12**, 703525 (2021).
51. Pedley, A. M. & Benkovic, S. J. A new view into the regulation of purine metabolism: the purinosome. *Trends Biochem. Sci.* **42**, 141–154 (2017).
52. He, Y. et al. Gut microbial metabolites facilitate anticancer therapy efficacy by modulating cytotoxic CD8$^+$ T cell immunity. *Cell Metab.* **33**, 988–1000.e7 (2021).
53. Suez, J. et al. Personalized microbiome-driven effects of non-nutritive sweeteners on human glucose tolerance. *Cell* **185**, 3307–3328.e19 (2022).
54. Afrizal, A. et al. Enhanced cultured diversity of the mouse gut microbiota enables custom-made synthetic communities. *Cell Host Microbe* **30**, 1630–1645.e25 (2022).
55. Xin, W. et al. Root microbiota of tea plants regulate nitrogen homeostasis and theanine synthesis to influence tea quality. *Curr. Biol.* **34**, 868–880.e6 (2024).
56. Heras-Murillo, I., Adán-Barrientos, I., Galán, M., Wculek, S. K. & Sancho, D. Dendritic cells as orchestrators of anticancer immunity and immunotherapy. *Nat. Rev. Clin. Oncol.* **21**, 257–277 (2024).
57. Garris, C. S. et al. Successful anti-PD-1 cancer immunotherapy requires T cell-dendritic cell crosstalk involving the cytokines IFN-gamma and IL-12. *Immunity* **49**, 1148–1161.e7 (2018).
58. Luu, M. et al. Microbial short-chain fatty acids modulate CD8$^+$ T cell responses and improve adoptive immunotherapy for cancer. *Nat. Commun.* **12**, 4077 (2021).
59. Wang, T. et al. Inosine is an alternative carbon source for CD8$^+$ T cell function under glucose restriction. *Nat. Metab.* **2**, 635–647 (2020).
60. Poyet, M. et al. A library of human gut bacterial isolates paired with longitudinal multiomics data enables mechanistic microbiome research. *Nat. Med.* **25**, 1442–1452 (2019).
61. Soto-Martin, E. C. et al. Vitamin biosynthesis by human gut butyrate-producing bacteria and cross-feeding in synthetic microbial communities. *mBio* **11**, e00886–00820 (2020).
62. Desai, M. S. et al. A dietary fiber-deprived gut microbiota degrades the colonic mucus barrier and enhances pathogen susceptibility. *Cell* **167**, 1339–1353.e21 (2016).
63. Watson, A. R. et al. Metabolic independence drives gut microbial colonization and resilience in health and disease. *Genome Biol.* **24**, 78 (2023).

64. Han, Y. et al. scRNA-seq profiling of neonatal and adult thymus-derived CD4$^+$ T cells by a T cell origin-time tracing model. *J. Mol. Cell. Biol.* **14**, mjac072 (2022).
65. Zeng, X. et al. Gut bacterial nutrient preferences quantified in vivo. *Cell* **185**, 3441–3456.e19 (2022).
66. Han, S. et al. A metabolomics pipeline for the mechanistic interrogation of the gut microbiome. *Nature* **595**, 415–420 (2021).
67. Xi, H. et al. A bacterial spermidine biosynthetic pathway via carboxyaminopropylagmatine. *Sci. Adv.* **9**, eadj9075 (2023).
68. Han, J., Lin, K., Sequeira, C. & Borchers, C. H. An isotope-labeled chemical derivatization method for the quantitation of short-chain fatty acids in human feces by liquid chromatography-tandem mass spectrometry. *Anal. Chim. Acta* **854**, 86–94 (2015).
69. Zhou, H. et al. A clinic responder-derived defined microbial consortium enhances anti-PD-1 immunotherapy efficacy in mice. *Zenodo* https://doi.org/10.5281/zenodo.18265182 (2026).

Acknowledgements

We thank X. Xu, S. Wang and W. Hu for technical assistance on metabolomic and proteomic analyses. This work was supported by the National Natural Science Foundation of China grant 82241228 (to Y.W. and C.Y.), 82241227 (to S.L.), 82030045 (to S.L.), 32230060 (to C.Y.), 31925001 (to C.Y.) and 82073152 (to L.X.); National Multi-disciplinary Treatment Project for Major Diseases 2020NMDTP (to S.L.); Shanghai Program for Outstanding Medical Academic Leader 2022LJ016 (to Y.W.); Collaborative Innovation Center for Clinical and Translational Science by Ministry of Education & Shanghai CCTS-202407PT (to S.L.) and CCTS-202508PT (to S.L.); Shanghai Chest Hospital Basic Research Project 2023YNKT-1 (to S.L.); and Shanghai Key Laboratory of Thoracic Tumor Biotherapy 2025SZ1710 (to S.L.).

Author contributions

C.Y., Y.W. and S.L. conceived the project. H.Z. performed most of the experiments, analysed data and wrote the paper. R.S. performed immunological analyses and some animal experiments. X.N. performed bioinformatic analysis and bacterial community design. L.X. collected and analysed clinical data. H.D. performed metagenomic sequencing on human faecal samples. Y.L. performed proteomic and metabolomic experiements and analysed the data. S.H. and W.D. provided technical assistance and essential materials. X.Z. and Y.Y. collected human samples. G.-P.Z. contributed to the experimental design and discussion. Y.W. and S.L. supervised tumour models and analysed data. C.Y. designed experiments, analysed data and wrote the paper.

Competing interests

C.Y., R.S., H.Z., Y.W. and S.L. have a patent pending related to this work (Chinese patent application number 2025110199804). The other authors declare no competing interests.

Additional information

Extended data is available for this paper at https://doi.org/10.1038/s41564-026-02279-6.

Supplementary information The online version contains supplementary material available at https://doi.org/10.1038/s41564-026-02279-6.

Correspondence and requests for materials should be addressed to Shun Lu, Ying Wang or Chen Yang.

Peer review information *Nature Microbiology* thanks Sean Gibbons, Hansoo Park and the other, anonymous, reviewer(s) for their contribution to the peer review of this work. Peer reviewer reports are available.

Reprints and permissions information is available at www.nature.com/reprints.

Publisher's note Springer Nature remains neutral with regard to jurisdictional claims in published maps and institutional affiliations.

[1]State Key Laboratory of Microbial Metabolism, and School of Life Sciences & Biotechnology, Shanghai Jiao Tong University, Shanghai, China. [2]Shanghai Institute of Immunology, Department of Immunology and Microbiology, Key Laboratory of Cell Differentiation and Apoptosis of Chinese Ministry of Education, Shanghai Jiao Tong University School of Medicine, Shanghai, China. [3]Shanghai Lung Cancer Center, Shanghai Key Laboratory of Thoracic Tumor Biotherapy, Shanghai Chest Hospital, Shanghai Jiao Tong University School of Medicine, Shanghai, China. [4]Department of Gastroenterology, Shanghai Key Laboratory of Pancreatic Diseases, Shanghai General Hospital, Shanghai Jiao Tong University School of Medicine, Shanghai, China. [5]CAS-Key Laboratory of Synthetic Biology, CAS Center for Excellence in Molecular Plant Sciences, Shanghai Institute of Plant Physiology and Ecology, Chinese Academy of Sciences, Shanghai, China. [6]Bio-Med Big Data Center, CAS Key Laboratory of Computational Biology, Shanghai Institute of Nutrition and Health, Chinese Academy of Sciences, Shanghai, China. [7]Shanghai Sixth People's Hospital Affiliated to Shanghai Jiao Tong University School of Medicine, Shanghai, China. [8]These authors contributed equally: Haiyan Zhou, Ruiming Sun, Xiaoqun Nie, Liliang Xia. ✉e-mail: shunlu@sjtu.edu.cn; ywangssmu@shsmu.edu.cn; yang.c@sjtu.edu.cn

https://doi.org/10.1038/s41564-026-02279-6

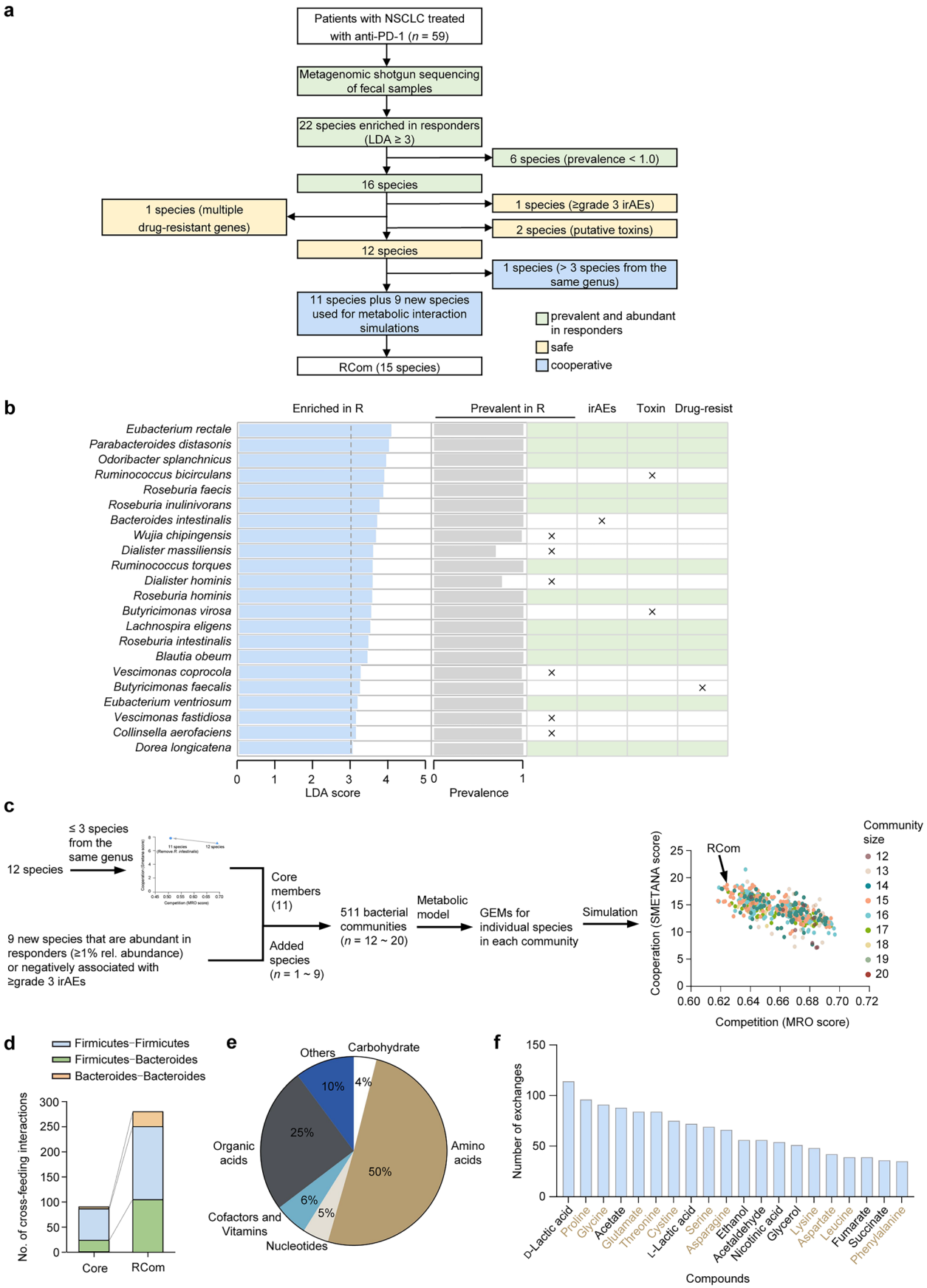

Extended Data Fig. 1 | See next page for caption.

https://doi.org/10.1038/s41564-026-02279-6

Extended Data Fig. 1 | Design of the defined bacterial consortium RCom. a, Schematic of the design process. The key criteria for selecting the 15 bacterial species for the RCom are shown in colored boxes. Based on metagenomic shotgun sequencing of faecal samples from anti-PD-1-treated NSCLC patients, the bacterial species enriched (LDA score ≥ 3.0) and prevalent (prevalence = 1.0) in the responder group were identified. For safety, the species associated with ≥grade 3 irAEs or harboring putative toxins or multiple drug-resistant genes were excluded. Lastly, a metabolically cooperative community was predicted based on metabolic interaction simulations. **b**, Selection of bacterial species based on enrichment and prevalence in responders and safety rule. The bacterial species that meet the criteria are shown in green boxes, whereas those excluded are denoted by bold X. **c**, Metabolic model-based prediction of interspecies interactions in bacterial communities. Calculated competition (MRO) and cooperation (SMETANA) scores for different sizes of bacterial communities are shown on the right. The SMETANA score was normalized by community size. Arrow indicates the RCom. **d**, Number of predicted intra- and inter-phylum cross-feeding interactions within the 11 core members and the RCom. **e**, Metabolite classes predicted to be exchanged between the RCom members. Compound classification is based on the Human Metabolome Database (HMDB). **f**, Top 20 potential cross-fed compounds in the RCom. Amino acids are indicated in brown.

https://doi.org/10.1038/s41564-026-02279-6

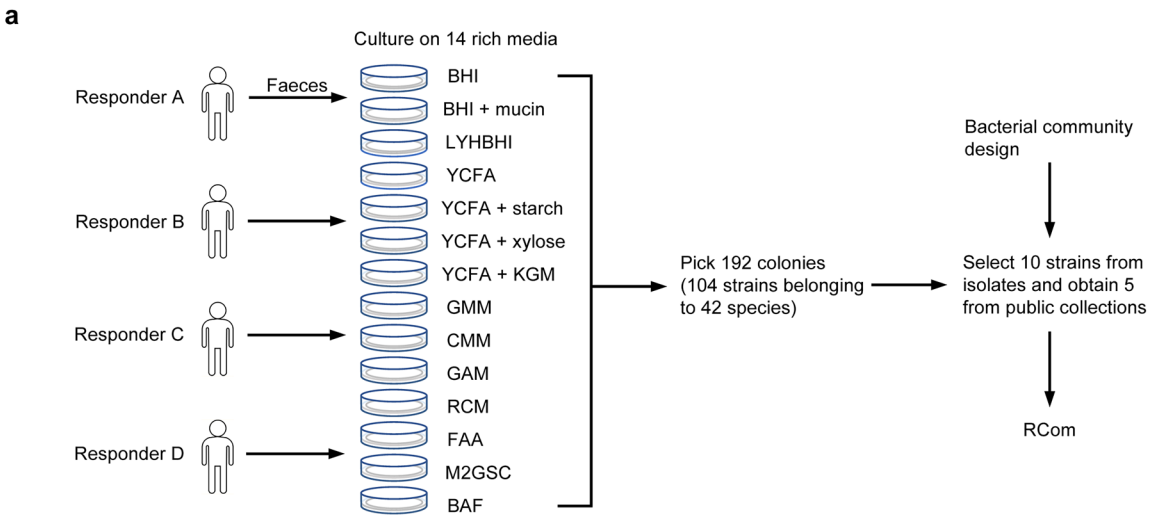

b

Strain	Genome (bp)	16S rRNA (bp)	Identity (%)	Closest strain	RCom	5 -mix	10 -mix-I	10 -mix-II	10 -mix-III
F2	4,483,529	1,419	99.14	*Odoribacter splanchnicus* DSM 20712	■	■		■	■
B5	5,062,925	1,380	99.79	*Parabacteroides distasonis* ATCC 8503	■	■		■	■
Y9	4,451,398	1,399	99.79	*Parabacteroides merdae* ATCC 43184	■	■		■	■
DSM 17242	3,734,239	1,394	100	*Alistipes finegoldii* DSM 17242	■	■		■	■
DSM 28863	2,304,821	1,398	100	*Alistipes inops* DSM 28863	■	■		■	■
YS7	2,569,141	1,393	99.49	*Eubacterium ventriosum* ATCC 27560	■		■		■
YS16	3,501,487	1,390	99.78	*Eubacterium rectale* ATCC 33656	■		■		■
LY17	3,417,702	1,395	99.50	*Blautia obeum* ATCC 27255	■		■		■
C10	3,056,315	1,410	99.57	*Ruminococcus torques* L2-14	■		■	■	
ATCC 27750	2,772,784	1,479	100	*Lachnospira eligens* ATCC 27750	■		■	■	
DSM 3992	3,545,964	1,403	100	*Dorea formicigenerans* DSM 3992	■		■	■	
DSM 13814	2,915,433	1,406	100	*Dorea longicatena* DSM 13814	■		■		■
LY8	3,410,569	1,412	99.43	*Roseburia hominis* A2-183	■		■	■	
LY20	3,736,947	1,413	99.15	*Roseburia inulinivorans* A2-194	■		■		■
YX27	4,392,341	1,389	99.28	*Roseburia faecis* M72/1	■		■	■	

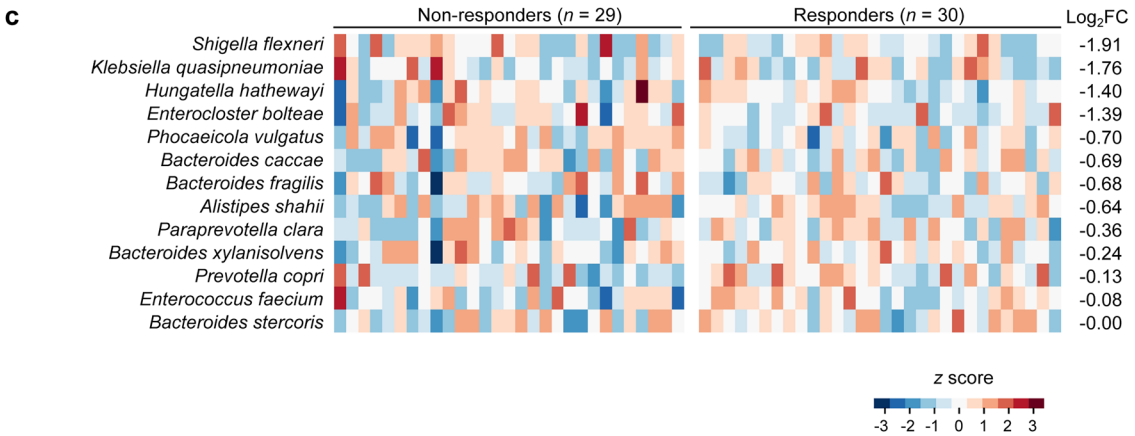

Extended Data Fig. 2 | Construction of the bacterial community RCom. a, Schematic showing the isolation of RCom members from faecal samples from anti-PD-1-responsive patients. **b**, A neighbor-joining phylogenetic tree of the 15 bacterial strains. Genome sequencing was conducted for the isolated 10 strains. Their closest reference strain was identified by comparing to the NCBI 16S ribosomal RNA sequence database. The RCom subsets (5-mix, 10-mix-I, 10-mix-II, and 10-mix-III) tested in vivo are indicated by colored boxes. **c**, For comparison, 13 bacterial strains were isolated from faecal samples from non-responder patients. Most of them are enriched in non-responders. Heatmap shows their relative abundances in responders versus non-responders among anti-PD-1-treated NSCLC patients as determined by metagenomic shotgun sequencing.

https://doi.org/10.1038/s41564-026-02279-6

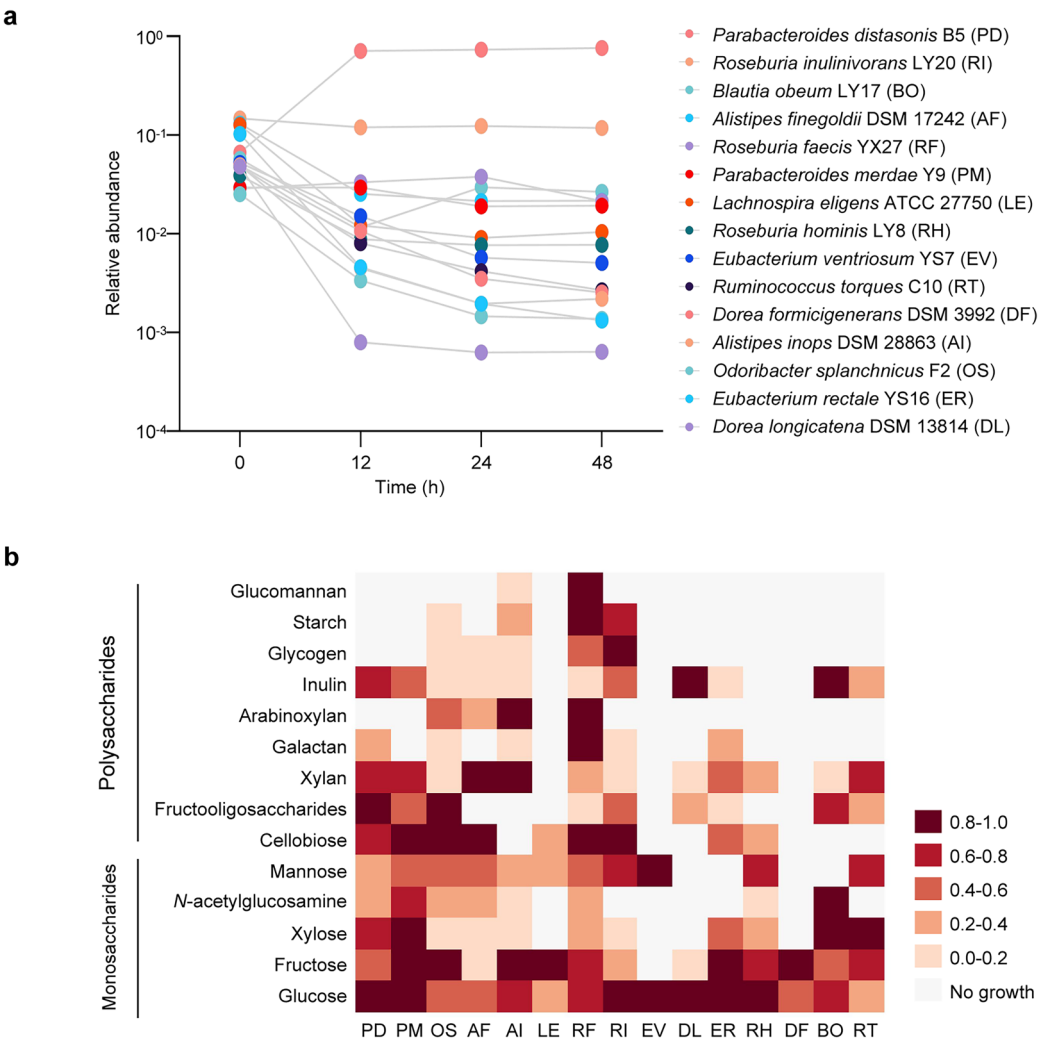

Extended Data Fig. 3 | Community growth and substrate utilization by the RCom members in vitro. a, The community reaches a stable composition quickly. The relative abundance of each strain was analyzed by qPCR. The two-letter abbreviations of the RCom members are indicated. **b**, Heat map showing carbohydrate utilization by each of the RCom members. The OD_{600} values are normalized to the maximum values within each strain and for the same substrate. Data shown in **a** and **b** are mean values from three biological replicates.

https://doi.org/10.1038/s41564-026-02279-6

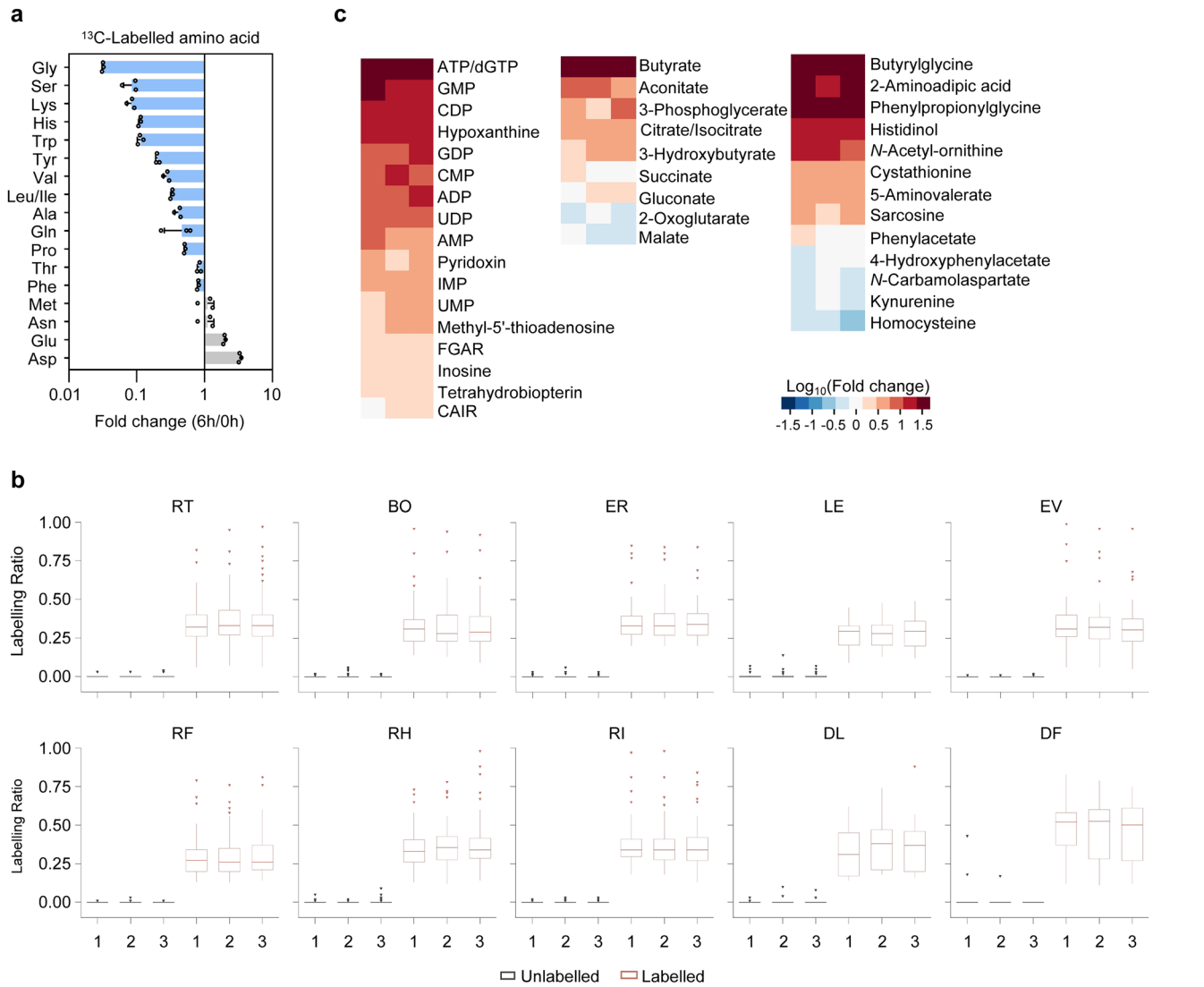

Extended Data Fig. 4 | Metabolic cross-feeding in the RCom as revealed by ^{13}C-proteomic and exometabolomic analyses. a, Five Bacteroidetes species were grown in a chemically defined medium containing ^{13}C-labelled or unlabelled glucose, and the spent medium was added to the culture of the 10-Firmicutes-species community. Extracellular concentrations of ^{13}C-labelled amino acids during cultivation of the Firmicutes community were measured by LC–MS and normalized to the values at the start of the culture (0 h). Data shown are mean ± s.d. ($n = 3$ independent experiments). **b**, Data shown are from three independent biological replicates from ^{13}C-labelled (orange) and unlabelled (black) spent medium experiments. The box plots depict the median, the upper and lower quartiles, and the rest of the distribution. Points that are 1.5 times the inter-quartile range beyond the upper and lower quartiles are considered outliers and shown individually. **c**, Heat map showing the changes in extracellular concentrations of metabolites after 6 h cultivation of the 10-Firmicutes-species community. The concentration values at 6 h are averaged from three independent experiments and normalized to the values at the start of the culture (0 h). The resulting fold changes ($\log_{10}$ transformed) are shown.

https://doi.org/10.1038/s41564-026-02279-6

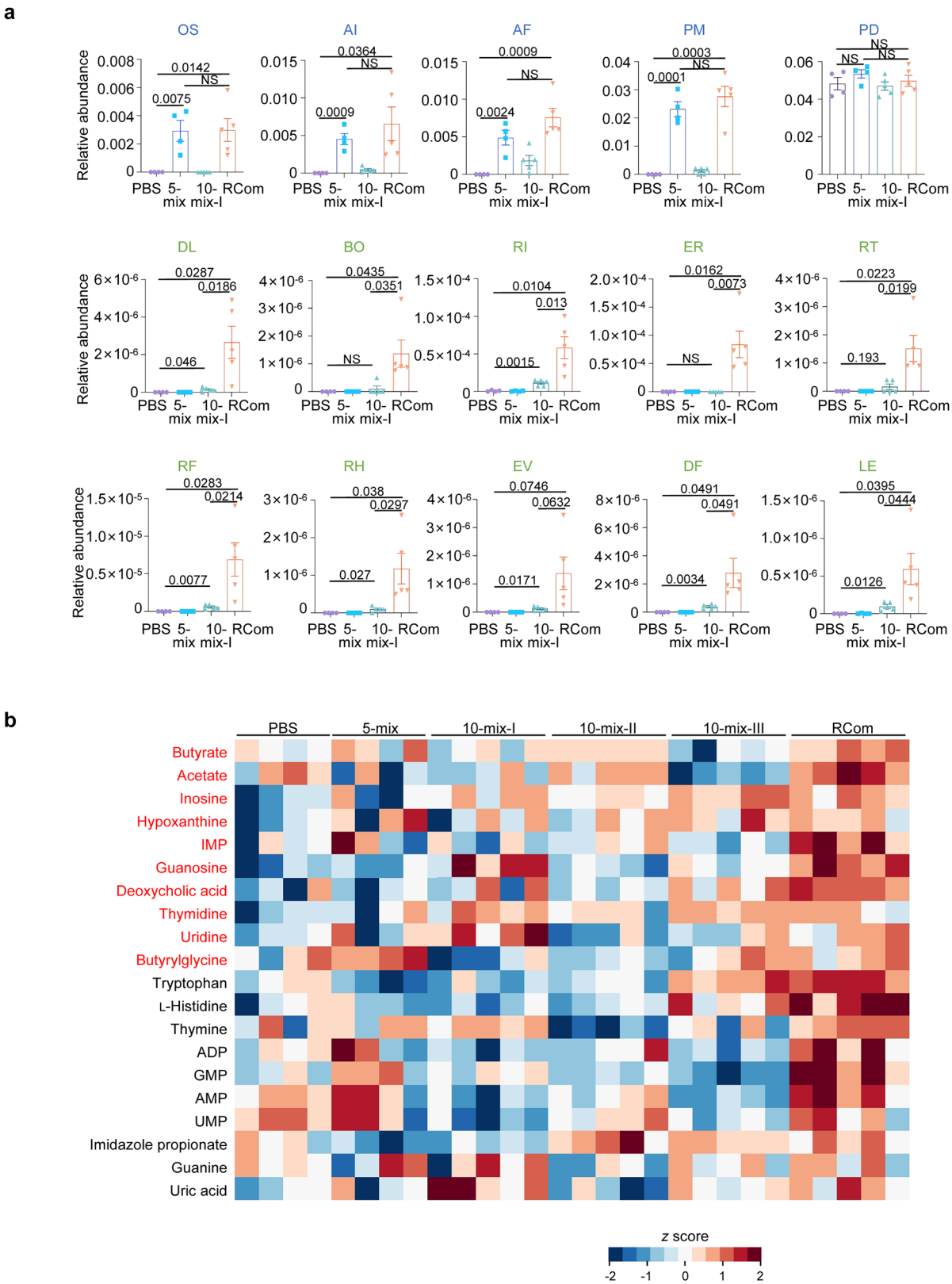

Extended Data Fig. 5 | Engraftment of the RCom in SPF mice. a, SPF mice were supplemented with the RCom ($n = 5$) or its subsets (PBS, $n = 4$; 5-mix, $n = 4$; 10mix-I, $n = 5$) daily by oral gavage for 7 days. The abundance of each of the 15 species in caecal samples was determined by qPCR and normalized to 16S rRNA level. Each species was denoted by two-letter abbreviation, and the color represents the phyla of the species (Bacteroidetes, blue; Firmicutes, green). **b**, Heat map showing the changed metabolites in the caecal content of mice supplemented with the indicated bacterial mixtures. Elevated metabolites in RCom- versus subset-supplemented mice are highlighted in red. Exact *P* values are provided in Source Data. Data in **a** are mean and s.e.m. Two-tailed unpaired *t*-test. NS, not significant.

https://doi.org/10.1038/s41564-026-02279-6

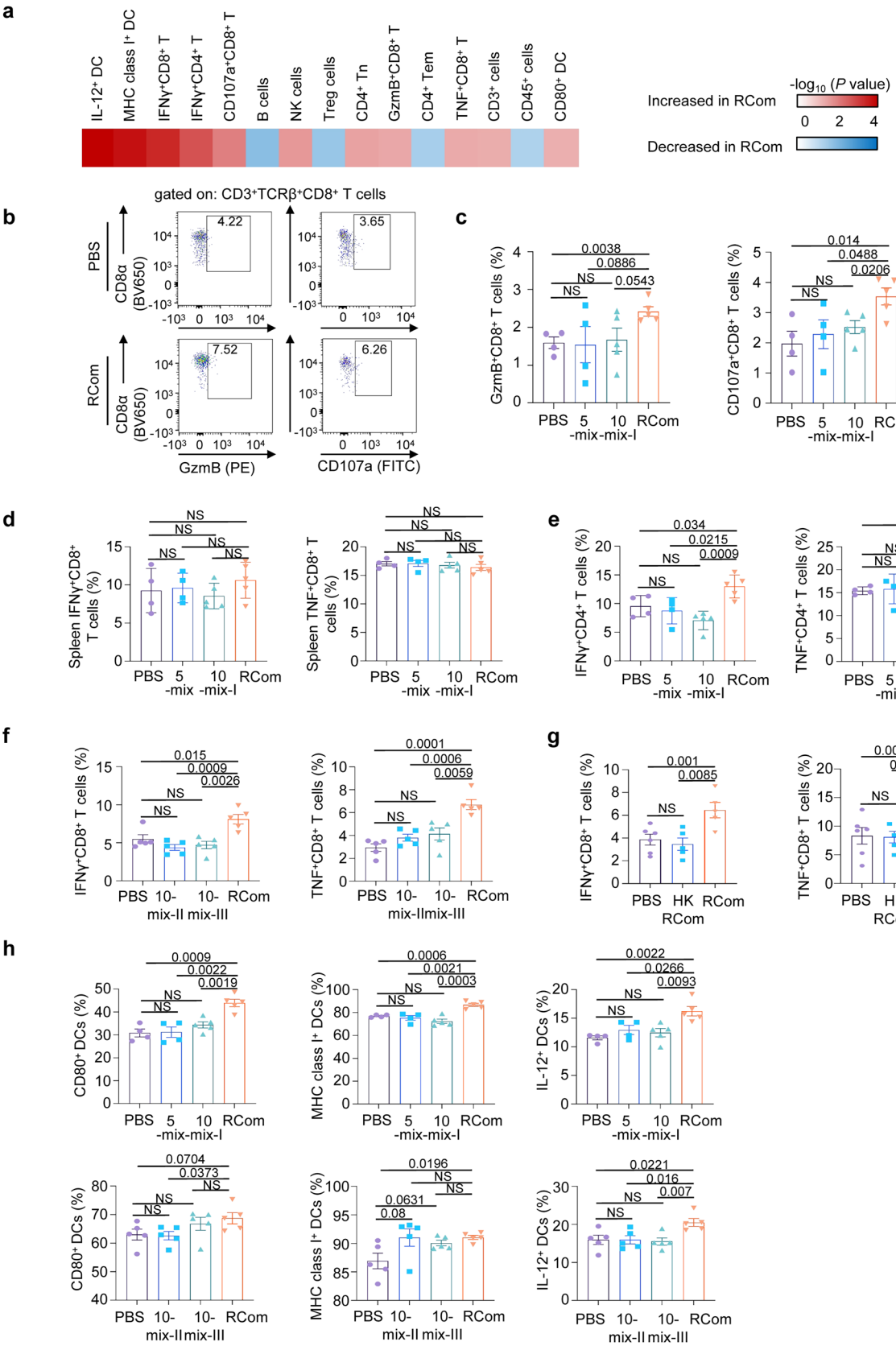

Extended Data Fig. 6 | See next page for caption.

https://doi.org/10.1038/s41564-026-02279-6

Extended Data Fig. 6 | RCom species act together to modulate colonic immune responses. a, SPF C57BL/6 mice were supplemented with bacterial mixtures or PBS daily by oral gavage for 7 days. The colonic lamina propria cells were analyzed by flow cytometry. Heat map showing the top 15 differentially abundant immune features between RCom- and PBS-supplemented mice. **b**, Representative flow cytometry plots show the expression of GzmB and CD107a by colonic $CD8^+$ T cells from RCom- or PBS-fed mice. **c**–**e**, Percentages of colonic $GzmB^+$ and $CD107a^+$ cells among $CD8^+$ T cells (**c**), splenic $IFN\gamma^+CD8^+$ and TNF^+CD8^+ T cells (**d**), or colonic $IFN\gamma^+CD4^+$ and TNF^+CD4^+ T cells (**e**) from mice supplemented with RCom ($n = 5$), its subsets 5-mix ($n = 4$) or 10-mix-I ($n = 5$), or PBS ($n = 4$). **f**,**g**, Percentages of $IFN\gamma^+$, TNF^+ of colonic $CD8^+$ T cells from mice supplemented with RCom subsets 10-mix-II or 10-mix-III (**f**) ($n = 5$ mice per group) or heat-killed (HK) RCom (**g**) (PBS, $n = 6$; HK, $n = 5$; RCom, $n = 5$). **h**, Percentages of $CD80^+$, MHC class I^+, and $IL\text{-}12^+$ of colonic DCs from mice supplemented with RCom or its subsets. PBS, $n = 4$ or 5; 5-mix, $n = 4$; 10-mix-I, 10-mix-II, 10-mix-III, RCom, $n = 5$ mice per group. Data in **c**–**h** are mean and s.e.m. Two-tailed unpaired *t*-test. NS, not significant.

https://doi.org/10.1038/s41564-026-02279-6

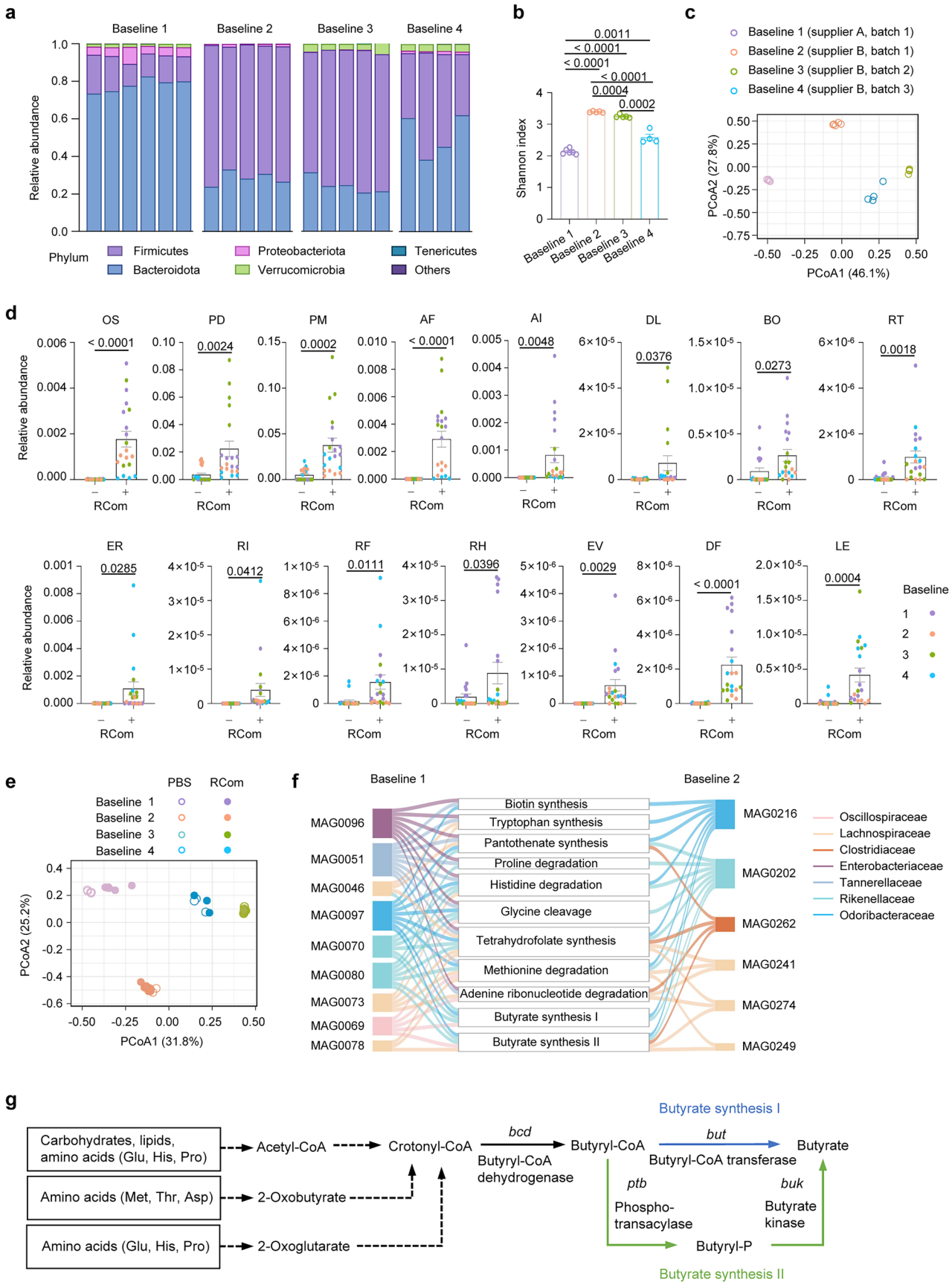

Extended Data Fig. 7 | See next page for caption.

https://doi.org/10.1038/s41564-026-02279-6

Extended Data Fig. 7 | RCom supplementation in mice harboring a variety of baseline gut microbiota. a, Four cohorts of SPF C57BL/6 mice were obtained from different commercial suppliers or the same supplier but in separate shipment batches. The baseline caecal microbiota were analysed by 16S rRNA sequencing. Phylogenetic composition of common bacterial taxa at the phylum level is shown. **b**, Alpha diversity of baseline caecal microbiota composition. **c**, Principal coordinate analysis (PCoA) of baseline microbiota composition using weighted UniFrac distances. **d**, Four cohorts of SPF C57BL/6 mice with different baseline gut microbiota were orally supplemented with RCom or PBS for 7 days. The abundance of each of the 15 species in caecal samples was determined by qPCR and normalized to 16S rRNA level. **e**, PCoA plot of caecal microbiota composition in RCom- and PBS-fed mice from the four cohorts. **f**, Metabolic modules and their encoding MAGs enriched in RCom- versus PBS-fed mice from two cohorts (baselines 1 and 2) as determined by metagenomic shotgun sequencing. MAGs were taxonomically classified according to NCBI RefSeq. **g**, Butyrate synthetic pathway in gut bacteria. Each circle in **b**–**e** represents an individual animal. Baseline 1: PBS, RCom, $n = 6$ mice per group; Baseline 2: PBS, RCom, $n = 5$ mice per group; Baseline 3: PBS, RCom, $n = 5$ mice per group; Baseline 4: PBS, RCom, $n = 4$ mice per group. Data shown in **b** and **d** are mean and s.e.m. Two-tailed unpaired *t*-test.

https://doi.org/10.1038/s41564-026-02279-6

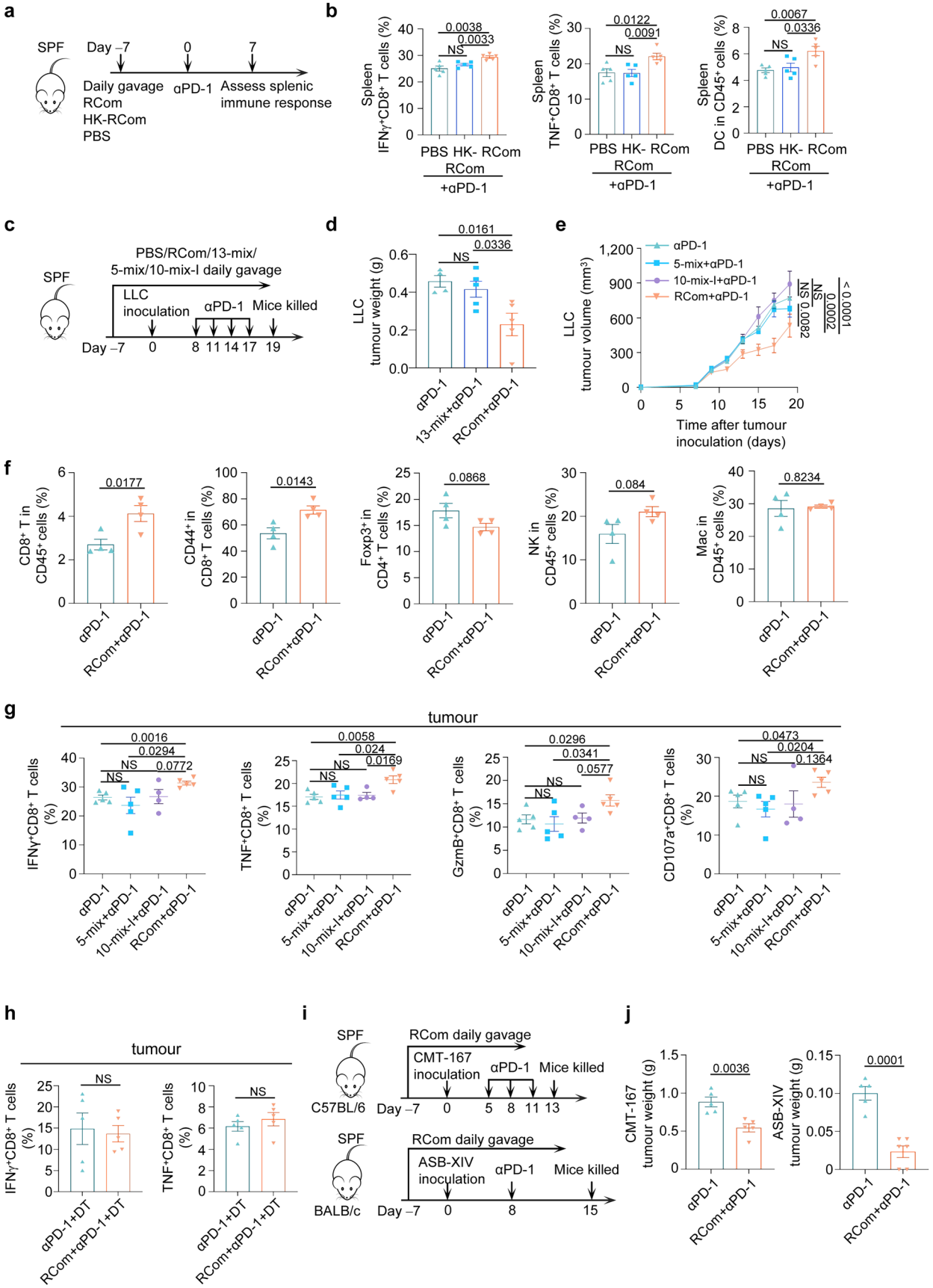

Extended Data Fig. 8 | See next page for caption.

https://doi.org/10.1038/s41564-026-02279-6

Extended Data Fig. 8 | RCom species act together to enhance anti-tumour immunity and anti-PD-1 efficacy. a,**b**, SPF C57BL/6 mice were i.p. injected with an anti-PD-1 antibody. Supplementation with RCom, heat-kiled (HK) RCom, or PBS daily by oral gavage started one week before anti-PD-1 treatment. Schematic of the experimental setup is shown (**a**). Percentages of IFNγ$^+$ and TNF$^+$ in CD8$^+$ T cells and DCs in CD45$^+$ cells in spleens from the mice were determined by flow cytometry (**b**) ($n = 5$ mice per group). **c**–**g**, SPF C57BL/6 mice were injected s.c. with LLC tumour followed by anti-PD-1 treatment. Supplementation of the indicated bacterial mixtures daily by oral gavage started one week before tumor inoculation. Schematic of the experimental setup is shown (**c**). Tumour weight at termination in PBS- ($n = 4$) or RCom- ($n = 5$) or 13-mix-fed ($n = 5$) mice (**d**) and tumor growth in mice supplemented with RCom- ($n = 5$) or 5-mix ($n = 5$) or 10-mix-I ($n = 4$) or PBS ($n = 5$) (**e**) were measured. Percentages of CD8$^+$ T cells in CD45$^+$ cells, CD44$^+$ cells in CD8$^+$ T cells, Foxp3$^+$ (Treg) cells in CD4$^+$ T cells, NK cells in CD45$^+$ cells, macrophage (Mac) in CD45$^+$ cells in the tumours (**f**) ($n = 4$ mice per group), IFNγ$^+$, TNF$^+$, GzmB$^+$, CD107a$^+$ among CD8$^+$ T cells in the tumour (**g**) (10-mix-I, $n = 4$; RCom, 5-mix, PBS, $n = 5$ mice per group) from mice supplemented with RCom or its subsets were determined by flow cytometry. **h**, Effect of DC depletion on proportions of IFNγ$^+$ and TNF$^+$ among CD8$^+$ T cells in the tumour from mice supplemented with RCom or PBS. DCs were depleted by i.p. injection of diphtheria toxin (DT). $n = 5$ mice per group. **i**,**j**, SPF C57BL/6 or BALB/c mice were injected s.c. with CMT-167 or ASB-XIV tumours followed by anti-PD-1 treatment. Supplementation of RCom or PBS daily by oral gavage started one week before tumour inoculation. Schematic of the experimental setup is shown (**i**) ($n = 5$ mice per group). Tumour weight of CMT-167 and ASB-XIV at termination was measured (**j**) (αPD-1, $n = 5$; RCom+αPD-1, $n = 6$). Data are mean and s.e.m. Two-way ANOVA (**e**) or two-tailed unpaired *t*-test (**b**, **d**, **f**–**h**, **j**). NS, not significant.

https://doi.org/10.1038/s41564-026-02279-6

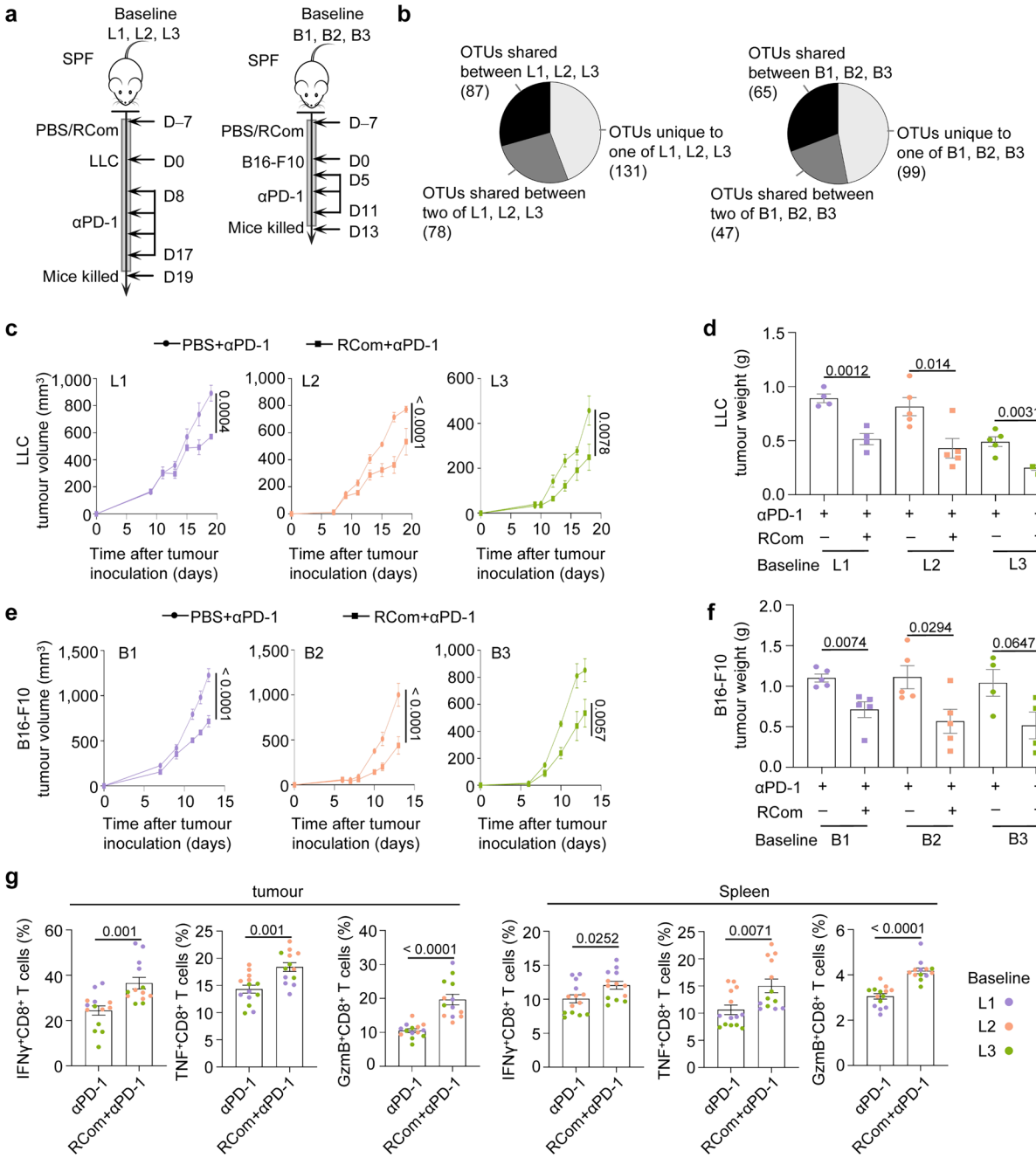

Extended Data Fig. 9 | Enhancement of anti-PD-1 efficacy by RCom was not influenced by baseline microbial variations. a, Schematic of the experimental setup. Three cohorts of SPF mice with different baseline gut microbiota (L1, L2, L3, and B1, B2, B3, respectively) were subject to inoculation of LLC or B16-F10 tumours followed by anti-PD-1 treatment. Daily administration of the RCom started one week before tumour inoculation. **b**, Shared and unique OTUs between the three baseline microbiota. **c**,**d**, LLC tumour growth curve (**c**) and tumour weight at termination (**d**) in the three cohorts of anti-PD-1 treated mice supplemented with RCom or PBS. **e**,**f**, B16-F10 tumour growth curve (**e**) and tumour weight at termination (**f**) in the three cohorts of anti-PD-1 treated mice supplemented with RCom or PBS. **g**, Percentages of IFNγ$^+$, TNF$^+$, and GzmB$^+$ cells among CD8$^+$ T cells in the LLC tumour and spleen of the three cohorts of mice, as determined by flow cytometry. L1: $n = 4$ mice per group; L2: $n = 5$ mice per group; L3: αPD-1, $n = 5$; RCom+αPD-1, $n = 4$. B1: $n = 5$ mice per group; B2: $n = 5$ mice per group; B3: $n = 4$ mice per group. Data are mean and s.e.m. Two-way ANOVA (**c**, **e**) or two-tailed unpaired *t*-test (**d**, **f**, **g**).

https://doi.org/10.1038/s41564-026-02279-6

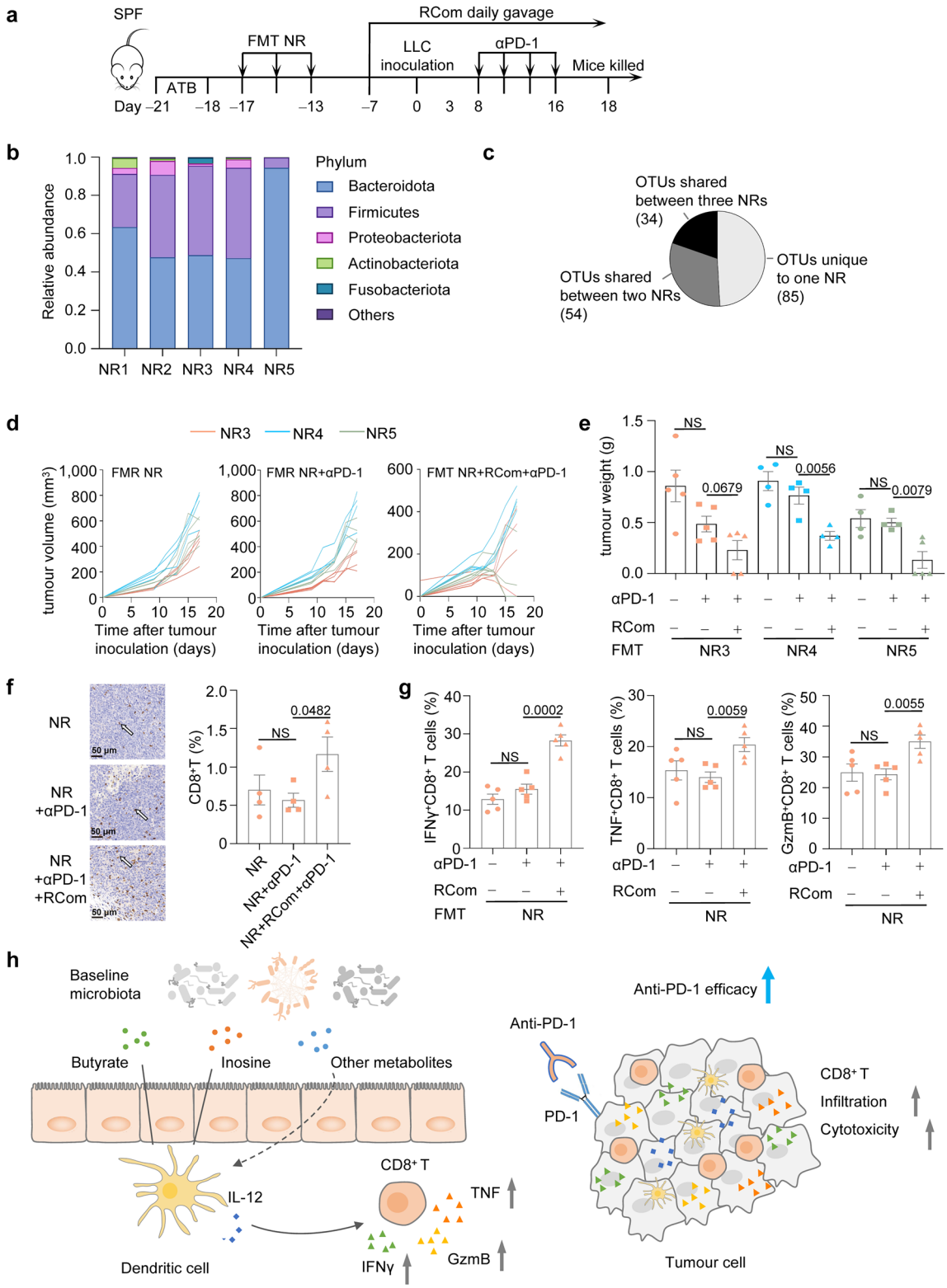

Extended Data Fig. 10 | See next page for caption.

https://doi.org/10.1038/s41564-026-02279-6

Extended Data Fig. 10 | RCom administration restores the anti-tumour activity of anti-PD-1 in mice with FMT from non-responder patients. a, Schematic of the experimental setup in the RCom prophylactic approach. FMT of faecal samples from three non-responder (NR) patients with NSCLC were individually performed in SPF C57BL/6 mice pretreated with ATB. Mice were inoculated with LLC tumour followed by injection of an anti-PD-1 antibody. Supplementation of the RCom or PBS daily by oral gavage started one week before tumour inoculation. **b**, Faecal microbial composition of NR donors analyzed by 16S rRNA sequencing. Phylogenetic composition of common bacterial taxa at the phylum level is shown. **c**, Shared and unique OTUs between the three NR patients (NR3, NR4, and NR5). **d**,**e**, LLC tumour growth curve (**d**) and tumour weight at termination (**e**) in RCom-supplemented and anti-PD-1-treated mice with FMT from individual NR donors. NR3: $n = 5$ mice per group; NR4: $n = 4$ mice per group; NR5: PBS, αPD-1, $n = 4$ mice per group, RCom+αPD-1, $n = 5$. **f**, IHC and quantification of $CD8^+$ T cells in LLC tumour from anti-PD-1 treated mice supplemented with RCom or PBS. Arrow indicates CD8 + T cells. $n = 4$ mice per group. **g**, Percentages of $IFN\gamma^+CD8^+$, TNF^+CD8^+, and $GzmB^+CD8^+$ T cells in the tumour of anti-PD-1 treated mice fed with RCom or PBS. $n = 5$ mice per group. Data are mean and s.e.m. Two-way ANOVA (d) or two-tailed unpaired t-test (**e**–**g**). ns, not significant. **h**, Despite a profound heterogeneity of the baseline gut microbiota, interspecies interactions within the RCom enabled its optimal engraftment and production of immunomodulatory metabolites including butyrate and inosine. Supplementation of the RCom increased intratumoral infiltration and cytotoxic activity of $CD8^+$ T cells, probably mediated by activation of DCs. Collectively, oral administration of the RCom robustly enhances the efficacy of anti-PD-1 cancer immunotherapy in preclinic models.

nature portfolio

Corresponding author(s): Chen Yang

Last updated by author(s): Jan 19, 2026

Reporting Summary

Nature Portfolio wishes to improve the reproducibility of the work that we publish. This form provides structure for consistency and transparency in reporting. For further information on Nature Portfolio policies, see our Editorial Policies and the Editorial Policy Checklist.

Statistics

For all statistical analyses, confirm that the following items are present in the figure legend, table legend, main text, or Methods section.

n/a	Confirmed	
☐	☒	The exact sample size (*n*) for each experimental group/condition, given as a discrete number and unit of measurement
☐	☒	A statement on whether measurements were taken from distinct samples or whether the same sample was measured repeatedly
☐	☒	The statistical test(s) used AND whether they are one- or two-sided *Only common tests should be described solely by name; describe more complex techniques in the Methods section.*
☒	☐	A description of all covariates tested
☒	☐	A description of any assumptions or corrections, such as tests of normality and adjustment for multiple comparisons
☐	☒	A full description of the statistical parameters including central tendency (e.g. means) or other basic estimates (e.g. regression coefficient) AND variation (e.g. standard deviation) or associated estimates of uncertainty (e.g. confidence intervals)
☒	☐	For null hypothesis testing, the test statistic (e.g. *F*, *t*, *r*) with confidence intervals, effect sizes, degrees of freedom and *P* value noted *Give P values as exact values whenever suitable.*
☒	☐	For Bayesian analysis, information on the choice of priors and Markov chain Monte Carlo settings
☒	☐	For hierarchical and complex designs, identification of the appropriate level for tests and full reporting of outcomes
☐	☒	Estimates of effect sizes (e.g. Cohen's *d*, Pearson's *r*), indicating how they were calculated

Our web collection on statistics for biologists contains articles on many of the points above.

Software and code

Policy information about availability of computer code

Data collection	The metabolomics data were collected by UltiMate 3000 UHPLc and quadrupole-orbitrap mass spectrometer (Q-Exactive, Thermo Fisher). The proteomics data were collected by an ultrahigh performance liquid chromatograph (EASY-nLC 1200, Thermo Fisher) coupled to a quadrupole–orbitrap mass spectrometer (Q Exactive HF-X, Thermo Fisher). FACS was performed by BD LSRFortessa X-20 (BD Biosciences, San Jose, CA). Clinical data were regularly collected by our collegues in Shanghai Chest hospital.
Data analysis	Statistical analyses were performed using GraphPad Prism (v.8.4.3) or SIMCA (for metabolomic analysis). The two-tailed unpaired Student's t-test (parametric) or two-tailed Mann-Whitney U test was used for all comparisons between two groups. Tumor growth curves were analyzed by two-way ANOVA. The Kaplan-Meier method was used to estimate progression-free survival (PFS) and overall survival (OS) of patients, with the differences between the groups calculated with the log-rank test. Hazard ratio (HR) from univariate Cox regression was used to determine the association between RCom abundance and PFS/OS. Details including statistical tests, exact value, and definition of n are provided in each figure legend.

For manuscripts utilizing custom algorithms or software that are central to the research but not yet described in published literature, software must be made available to editors and reviewers. We strongly encourage code deposition in a community repository (e.g. GitHub). See the Nature Portfolio guidelines for submitting code & software for further information.

Data

Policy information about availability of data

All manuscripts must include a data availability statement. This statement should provide the following information, where applicable:

- Accession codes, unique identifiers, or web links for publicly available datasets
- A description of any restrictions on data availability
- For clinical datasets or third party data, please ensure that the statement adheres to our policy

Whole-genome shotgun sequencing data of human fecal samples (accession number PRJNA1195622), genomic sequences of the 10 isolated strains (PRJNA1312235), 16S rRNA (PRJNA1193840) and whole-genome shotgun sequencing data (PRJNA1196516) of mouse cecal samples have been deposited in the NIH Sequence Read Archive (SRA). The proteomics data have been deposited in the PRIDE repository (PXD064618). Source data are provided with this paper. The codes for metabolic interaction analysis and Cox regression analysis of survival generated during this study are available at GitHub: http://github.com/zhouhaiyan5555/RCom.

Research involving human participants, their data, or biological material

Policy information about studies with human participants or human data. See also policy information about sex, gender (identity/presentation), and sexual orientation and race, ethnicity and racism.

Reporting on sex and gender	The outcomes were consistent across sexes. Therefore, we have chosen not to delineate the results by these factors to avoid undue emphasis on distinctions that were not meaningful in the context of our study.
Reporting on race, ethnicity, or other socially relevant groupings	In this study, no distinction of race or ethnicity was made at any point in the collection of human fecal samples or any other analysis.
Population characteristics	Human fecal samples were obtained from Chinese immunotherapy patients, the detail information were provided in Supplementary Table 1, 6 and 15.
Recruitment	Fecal samples were collected from patients with informed consent at Shanghai Chest Hospital affiliated to Shanghai Jiao Tong University between October 2016 and July 2023.
Ethics oversight	Feces were collected before the anti-PD-1 treatment according to the study protocol approved by the Ethics Committee of Shanghai Chest Hospital (approval number KS23014-A).

Note that full information on the approval of the study protocol must also be provided in the manuscript.

Field-specific reporting

Please select the one below that is the best fit for your research. If you are not sure, read the appropriate sections before making your selection.

☒ Life sciences ☐ Behavioural & social sciences ☐ Ecological, evolutionary & environmental sciences

For a reference copy of the document with all sections, see nature.com/documents/nr-reporting-summary-flat.pdf

Life sciences study design

All studies must disclose on these points even when the disclosure is negative.

Sample size	No statistical methods were used to determine sample size for experiments in the manuscript. We followed protocols and reasonable sample sizes from previously published studies.
Data exclusions	No data were excluded from analyses.
Replication	All attempts at replication were successful. At least three independent replications were carried out for each quantification analysis.
Randomization	Mice were randomly assigned to different experimental groups and no animals were excluded from the analyses.
Blinding	Data collection and analysis were not performed blind to the conditions of the experiments.

Reporting for specific materials, systems and methods

We require information from authors about some types of materials, experimental systems and methods used in many studies. Here, indicate whether each material, system or method listed is relevant to your study. If you are not sure if a list item applies to your research, read the appropriate section before selecting a response.

Materials & experimental systems

n/a	Involved in the study
☐	☒ Antibodies
☐	☒ Eukaryotic cell lines
☒	☐ Palaeontology and archaeology
☐	☒ Animals and other organisms
☒	☐ Clinical data
☒	☐ Dual use research of concern
☒	☐ Plants

Methods

n/a	Involved in the study
☒	☐ ChIP-seq
☐	☒ Flow cytometry
☒	☐ MRI-based neuroimaging

Antibodies

Antibodies used

Antibodies for mice analysis:
Fixable viability stain 510(BD Biosciences, Cat# 564406, RRID: AB_2869572, 1:1000)
rat anti-mouse CD45, clone 30-F11, AF700 conjugated(Invitrogen, Cat# 56-0451-82; RRID: AB_396774, 1:400)
hamster anti-mouse CD3e, clone 145-2C11, BV711 conjugated(BD Biosciences, Cat# 563123; RRID: AB_2687954, 1:400)
rat anti-mouse CD8a, clone 53-6.7, BV650 conjugated(Biolegend, Cat# 100742; RRID: AB_2563056, 1:400)
rat anti-mouse CD4, clone GK1.5, BV786 conjugated(BD Biosciences, Cat# 563331; RRID: AB_2738140, 1:400)
hamster anti-mouse TCRβ, clone H57-597, PerCP-CyTM5.5 conjugated(Biolegend, Cat# 109227; RRID: AB_1575176, 1:400)
rat anti-mouse CD44, clone IM7, BV785 conjugated(Biolegend, Cat# 103059; RRID: AB_2571953, 1:400)
rat anti-mouse CD62L, clone MEL-14, APC-R700 conjugated(BD Biosciences, Cat# 565159; RRID: AB_2737397, 1:600)
mouse anti-mouse NK1.1, clone PK136, FITC conjugated(eBioscience, Cat# 11-5941-82; RRID: AB_465318, 1:400)
rat anti-mouse CD183 (CXCR3), clone S18001A, Brilliant Violet 421TM conjugated(Biolegend, Cat# 155907; RRID: AB_2832543, 1:400)
rat anti-mouse Foxp3, clone FJK-16S, APC conjugated(Invitrogen, Cat# 17-5773-82; RRID: AB_469457, 1:400)
rat anti-mouse IFN-γ, clone XMG1.2, Brilliant Violet 421TM conjugated(Biolegend, Cat# 505829; RRID: AB_10897937, 1:400)
rat anti-mouse TNF alpha, clone MP6-XT22, PE-Cyanine7 conjugated(eBioscience, Cat# 25-7321-82; RRID: AB_11042728, 1:400)
rat anti-mouse CD107a, clone 1D4B, FITC conjugated(BD Biosciences, Cat# 553793; RRID: AB_395057, 1:400)
rat anti-mouse Granzyme B, clone NGZB, PE conjugated(Invitrogen, Cat# 12-8898-82; RRID: AB_10870787, 1:400)
mouse anti-human Ki-67, clone B56, PerCP-CyTM5.5 conjugated(BD Biosciences, Cat# 561284; RRID: AB_10611574, 1:400)
rat anti-mouse CD45R/B220, clone RA3-6B2, PerCP-CyTM5.5 conjugated(BD Biosciences, Cat# 552771; RRID: AB_394457, 1:400)
rat anti-mouse CD11b, clone M1-70, APC-R700 conjugated(Biolegend, Cat# 101222; RRID: AB_493705, 1:600)
hamster anti-mouse CD11c, clone N418, BV785 conjugated(Biolegend, Cat# 117335; RRID: AB_11219204, 1:400)
rat anti-mouse F4/80, clone T45-2342, BV421 conjugated(BD Biosciences, Cat# 565411; RRID: AB_2734779, 1:400)
rat anti-mouse IA/IE MHC-II, clone M5/114.15.2, PerCP-CyTM5.5 conjugated(BD Biosciences, Cat# 562363; RRID: AB_11153297, 1:400)
rat anti-mouse CD86, clone GL-1, PE conjugated(BD Biosciences, Cat# 553692; RRID: AB_394994, 1:400)
hamster anti-mouse CD80, clone 16-10A1, APC conjugated(Biolegend, Cat# 104713; RRID: AB_313134, 1:400)
mouse anti-mouse H-2Kd/H-2Dd, clone 34-1-2S, PE-Cyanine7 conjugated(Biolegend, Cat# 114717; RRID: AB_2749955, 1:400)
rat anti-mouse IL-12/IL-23 p40, clone C15.6, APC/FireTM 750 conjugated(Biolegend, Cat# 505217; RRID: AB_2928031, 1:200)
rat anti-mouse Ly-6G, clone 1A8, BV786 conjugated(BD Biosciences, Cat# 569406; RRID: AB_3685040, 1:400)
rat anti-mouse Siglec F, clone E502440, Brilliant Violet 421TM conjugated(BD Biosciences, Cat# 565934; RRID: AB_2722581, 1:400)

Antibodies for mice treatment:
InVivoMab anti-mouse PD-1 (CD279), clone RMP1-14(BioXCell, Cat# BE0146; RRID: AB_10949053), 200ug/mice
InVivoMab anti-mouse CD8α, clone 2.43(BioXCell, Cat# BE0061; RRID: AB_1125541), 100ug/mice
InVivoMAb rat IgG2a isotype control, anti-trinitrophenol, clone 2A3(BioXCell, Cat# BE0089; RRID: AB_1107769), 200ug/mice

Antibodies for immunohistochemistry:
Recombinant anti-CD8 alpha Rabbit mAb(Servicebio, Cat# GB15068; RRID: AB_3431943)
HRP-labeled goat anti-mouse IgG(Servicebio, Cat# GB23301; RRID: AB_2904020)

Validation

All the antibodies are commercially available. Quality validations were performed by each manufacturer.

Eukaryotic cell lines

Policy information about cell lines and Sex and Gender in Research

Cell line source(s)

Lewis lung cancer (LLC) cells were purchased from ATCC, Cat# CRL-1642
B16-F10 cells were purchased from ATCC, Cat# CRL-6475
MC38 cells were purchased from ATCC, Cat# AC337600
CMT-167 lung adenocarcinoma cells (Cat# BFN60808932) and ASB-XIV pulmonary squamous carcinoma cells (Cat# BFN60904188) were purchased from Shanghai Bluefbio Biology Technology Development Co., Ltd. (China)

Authentication

Cell lines were authenticated by the vendor and no further authentication in the laboratory.

Mycoplasma contamination

Cells were not tested for mycoplasma contamination.

Commonly misidentified lines
(See ICLAC register)

No commonly misidentified lines were used in this study.

Animals and other research organisms

Policy information about studies involving animals; ARRIVE guidelines recommended for reporting animal research, and Sex and Gender in Research

Laboratory animals	Specific pathogen-free 6 to 8 week old female C57BL/6 mice were supplied by Charles River Laboratories and Shanghai Lingchang Biotechnology, SPF female BALB/c mice and B-Cd11c-EGFP-DTR-Luc mice (6–8 weeks old) were purchased from Shanghai Lingchang Biotechnology and Biocytogen (China), respectively. These mice were housed in an animal facility in accordance with protocols approved by the Institutional Animal Care of Use Committee of Shanghai Jiao Tong University.
Wild animals	no wild animals were used in the study
Reporting on sex	To minimize variability and facilitate randomisation, only females were used in the findings reported in this paper. Plans will be made to confirm these results in males.
Field-collected samples	no field collected samples were used in the study
Ethics oversight	All animal experiments were approved by the Institutional Animal Care of Use Committee of Shanghai Jiao Tong University (IACUC number: A2025207).

Note that full information on the approval of the study protocol must also be provided in the manuscript.

Plants

Seed stocks	N/A
Novel plant genotypes	N/A
Authentication	N/A

Flow Cytometry

Plots

Confirm that:

☒ The axis labels state the marker and fluorochrome used (e.g. CD4-FITC).

☒ The axis scales are clearly visible. Include numbers along axes only for bottom left plot of group (a 'group' is an analysis of identical markers).

☐ All plots are contour plots with outliers or pseudocolor plots.

☒ A numerical value for number of cells or percentage (with statistics) is provided.

Methodology

Sample preparation	All protocols of the flow cytometry related experiments are described in detail in the “Methods" section.
Instrument	BD LSRFortessa X-20 (BD Biosciences, San Jose, CA).
Software	Data were analyzed with FlowJo software.
Cell population abundance	The fluorescence levels of at least 100,000 cells were measured.
Gating strategy	Detailed strategy were described in supplementary figure 6.

☒ Tick this box to confirm that a figure exemplifying the gating strategy is provided in the Supplementary Information.